Chapter 1

Introductory Chapter: Iridium Complexes as Organic Light Emitting Diodes (OLEDs): A Theoretical Analysis

Ruby Srivastava

Additional information is available at the end of the chapter

http://dx.doi.org/10.5772/intechopen.78398

1. Introduction

A specific discipline of electronics, which focus on light-emitting or light-detecting devices, the term "Optoelectronics" is used in the broader perspective. Such devices include those that emit light (LEDs and light bulbs), channel light (fiber optic cables), detect light (photodiodes and photoresistors), or are controlled by light (optoisolators and phototransistors). An interesting combination of electronics and optics, Optoelectronics find varied applications in telecommunications, military services, medical field, solid state devices (sensors, IR emitters, and laser emitters), and automatic control systems. The other counterparts as photo resistors and photovoltaic devices are also used for various applications. Nowadays, photodetectors has confronted significant challenges regarding the realization of efficient and sensitive detection with low-noise for the ultraviolet (UV), visible, and infrared regimes of electromagnetic spectrum.

Cyclometalated Ir(III) complexes are used as the organic light emitting diode (OLED) phosphors due to the phosphorescent emission, which spans the whole visible spectrum. These complexes are the most effective and tunable phosphorescent material for OLED devices due to their higher internal quantum efficiency compared to the fluorescent ones (3, 1) [1, 2]. These complexes can be used as photocatalysts for CO_2 reduction, catalysts for chemical reactions. Biological reagents and photo-oxidants: Few parameters which can lead to the success of these complexes are emission, color tunability, stability, strong spin-orbit coupling, triplet quantum yield, and efficiency toward the radiative transitions. Studies on the homoleptic and heteroleptic iridium complexes are carried out in the absorption spectrum, which lies in the UV-visible region (**Figure 1**).

The synthesis and photophysics of Ir(III) complexes have been of great interest as OLEDs as these complexes represent the most effective, tunable, and sublimable phosphorescent materials.

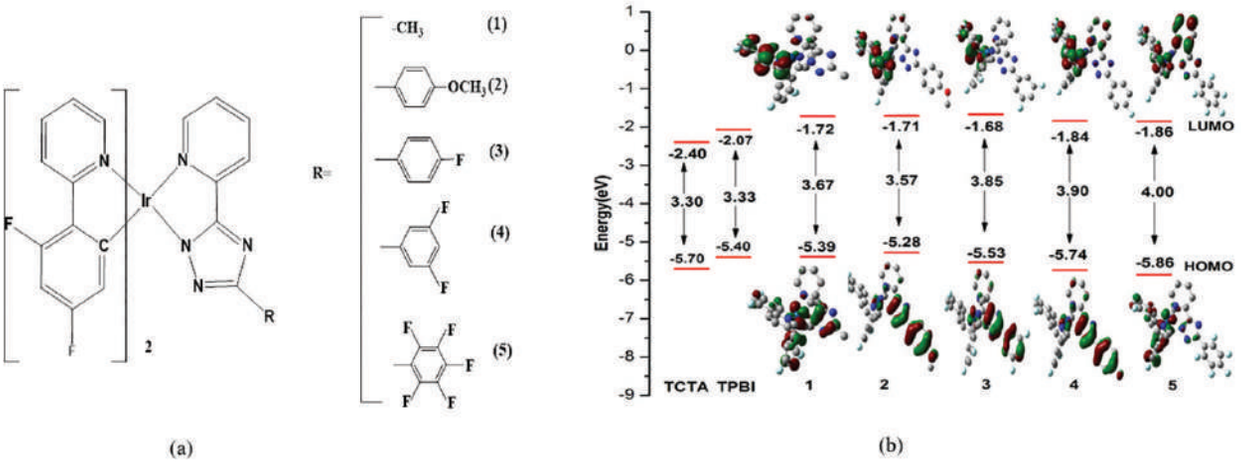

Figure 1. (a) Illustration of five Ir complexes and (b) a pictorial representation of energy highest occupied molecular orbital (HOMO), lowest unoccupied molecular orbital (LUMO) of the given complexes along with the host materials (Tris(4-carbazoyl-9-ylphenyl)amine (TCTA) and 2,2′,2″-1,3,5-Tris(1-phenyl-1H-benzimidazol- 2-yl)benzene (TPBI)).

OLEDs are also utilized as sensors, probes, imaging agents, and photosensitizers for electron and energy transfer. Till now the fabrication of red and green emitting Ir(III) complexes have been successfully fabricated with high-quantum efficiencies, but achieving phosphorescence with high-quantum efficiency for blue light emitting OLEDs is still a challenge. Therefore, several strategies have been developed on how to shift the emission to a blue color. Apart from experimental results theoretical results have been taken to measure the efficiency of blue OLEDs by computational methodologies. Therefore, here we will discuss the theoretical methodology used in design complexes to predict the blue color.

2. Theoretical measurements

The theoretical measures are initialed by the geometrical stability of the electronic structures of these complexes, the nature-type as well as the percentage molecular orbital contributions from the different ligands, absorption spectra in solvent, and the evaluation of excited state lifetimes. Later on, evaluation of the spin-orbital coupling (SOC) matrix element and the predictive measurements are used to calculate the radiative rate constant k_r, and lastly the phosphorescent properties and the better performance of the OLED are discussed, which include the charge injection/transport and balance ability, the energy transfer rate, and triplet exciton confinement for host and guest materials [3]. In some design complexes, two host materials are also suggested for device structure comparing their triplet energies and charge transport properties for the studied guest complexes [4] (**Figure 2**).

The ionization potential (IP), electron affinity (EA), hole extraction potential (HEP), electron extraction potential (EEP), reorganization energy (λ), and HOMO-LUMO gap (HL) HOMO (highest occupied molecular orbital) and LUMO (lowest unoccupied molecular orbital) are calculated by Gaussian and ADF software. The basis sets and functional are used as per requirements of the design complexes.

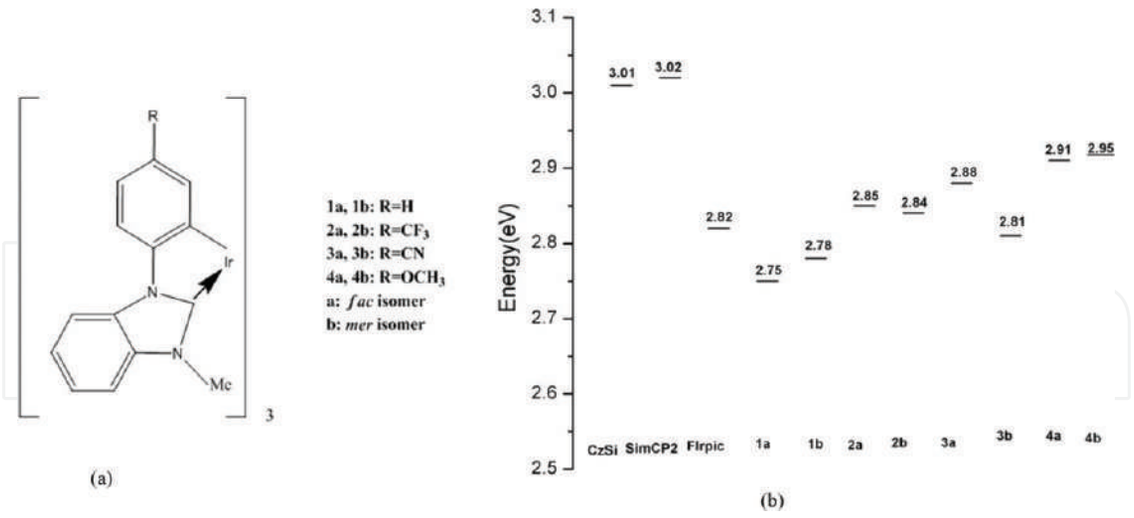

Figure 2. (a) Illustration of eight Ir complexes and (b) triplet energy representation of the eight complexes along with the triplet energy of host materials (CzSi, SimCP2, and FIrpic).

3. Results

The first step is to look into the ground state electronic structures, as the observed differences in the optoelectronic and photophysical properties depend on the electronic structures. Frontier molecular orbital (FMO) also plays a key role in gaining a better understanding of the optical and chemical properties. A detailed examination of the pertinent orbitals is carried out to see the HOMO and LUMO energies. For the singlet-triplet transitions, it is easy to take the first 10 leading excited states (with CI coefficients) and the first triplet energy states. On the basis of the optimized structures in the excited state, the emission spectra of the considered molecules are investigated. The good performance of an OLED device depends on the charge mobilities and a comparable balance between the hole and electron transport, it is necessary to calculate the charge injection properties as ionization potentials (IPs), electron affinities (EAs), HOMO and LUMO, reorganization energy, hole and electron extraction potentials (HEP, EEP). For the photoluminescent materials, it is anticipated that lower the IP of the emitter, the easier the entrance of holes from the hole-transport layer (HTL) to the emitter, and the higher the EA of the emitter, the easier the entrance of electrons from the electron-transport layer (ETL). Solvent polarization energy (SPE) is also used to estimate the self-trapping energies of charge in the materials, which is the energy due to the structural relaxation. The studies of the guest-host relationship are also important as the efficiency of OLEDs is improved on the basis of these investigations. As iridium phosphors have to be widely spread into the host matrix, a relatively long phosphorescence time for metal complexes can cause a long range of exciton diffusion, which may lead to dominant triplet-triplet annihilation. This will get quenched in the adjacent layers of materials in OLEDs. Here it is to mention that an effective host material is very important to achieve efficient electrophosphorescence. Several other requirements for the effective host material are (a) HOMOs and the LUMOs of the host material should match those of neighboring

active layers to lower the device driving voltage and reduce the hole and electron injection barrier. (b) The host should possess higher triplet energies than those of the dopant emitters so as to confine the triplet excitons in the emissive layer and to prevent reverse energy transfer from the guest back to the host. (c) The charge carrier transport properties of the host have to be good and it should balance the hole-electron recombination process. Dexter energy transfer also plays a significant role in obtaining the triplet excitons for the guest materials and the corresponding rate is correlated with the changes in Gibbs free energy (triplet energy difference) based on the Marcus electron-transfer theory.

Thus, we can say that though the OLED development is more of an experimental field than being a theoretically determined science. Nevertheless, the key parameters discussed here can be reliably considered in the theory and this knowledge will surely help in the design and fabrication of new phosphorescent OLEDs.

Acknowledgements

I acknowledge the financial assistance by the DST WOS A project (SR/WOS A/CS-1005/2014). I am also thankful to my Mentor Dr. G. Narahari Sastry, Center for Molecular Modeling, CSIR-Indian Institute of Chemical Technology for the support.

Author details

Ruby Srivastava

Address all correspondence to: amitruby1@gmail.com

CSIR-IICT, Hyderabad, India

References

[1] Srivastava R, Laxmikanth Rao J, Kotamarthi B. Theoretical study of electronic structures and opto-electronic properties of iridium(III) complexes containing benzoxazole derivatives and different ancillary β-diketonate ligands. Computational and Theoretical Chemistry. 2014;**1035**:51-59. DOI: 10.1016/j.comptc.2014.02.026

[2] Srivastava R, Kada Y, Kotamarthi B. Theoretical studies of electronic structures and opto-electronic properties of blue emitting heteroleptic Iridium(III) complexes containing 1,1 dithiolates. Computational and Theoretical Chemistry. 2013;**1009**:35-42. DOI: 10.1016/j.comptc.2012.12.032

[3] Srivastava R, Laxmikanth Rao J. The effect of substituted 1,2,4-triazole moiety on the emission, phosphorescent properties of the blue emitting heteroleptic Iridium(III) complexes and the OLED performance: A theoretical study. Physical Chemistry Chemical Physics. 2014;**16**:17284. DOI: 10.1039/c4cp02368d

[4] Srivastava R. The effect of substituted moiety on the optoelectronic and photophysical properties of tris (phenyl benzimidazolinato) Ir(III) carbene complexes and the OLED performance: A theoretical study. Molecular Physics. 2015;**113**(12):1451-1464. DOI: 10.1080/00268976.2014.1002824

IntechOpen

Chapter 2

Monolithically Integrable Si-Compatible Light Sources

Jesús Alarcón-Salazar, Liliana Palacios-Huerta,
Alfredo Abelardo González-Fernández,
Alfredo Morales-Sánchez and
Mariano Aceves-Mijares

Additional information is available at the end of the chapter

http://dx.doi.org/10.5772/intechopen.75116

Abstract

On the road to integrated optical circuits, the light emitting device is considered the bottleneck preventing us from arriving to the fully monolithic photonic system. While the development of silicon photonics keeps building momentum, the indirect bandgap nature of silicon represents a major problem for obtaining an integrated light source. Novel nanostructured materials based on silicon, such as silicon-rich oxide (SRO) containing silicon nanoparticles, present intense luminescence due to quantum phenomena. Using this material, electroluminescent devices have already been fabricated and even integrated in monolithic photonic circuits by fully complementary metal oxide semiconductor (CMOS) compatible techniques, opening the door to seamless electronic and photonic integration. The present work discusses some of the strategies used to improve the performance of SRO-based electroluminescent devices fully compatible with CMOS technology. Results from the characterization of devices obtained using different approaches are presented and compared.

Keywords: silicon-rich oxide, silicon nanoparticles, light emitting capacitor, photonic system, monolithic integration

1. Introduction

There are many research groups devoting their efforts to contribute to the development of a fully integrated photonic lab-on-a-chip (LOC) that can take advantage of the use of silicon (Si) as the main material. These are, among others, large availability and low cost of the material, a very well-established fabrication and testing ecosystem, the existence of a fabless model, very large chip fabrication volumes and yields, the possibility of testing using parallel

systems, seamless integration with electronics, etc. All these advantages have driven a significant advancement in the past years regarding the development of Si-based LOC systems and, in particular, in silicon photonics. However, there still are important barriers to overcome that have prevented the transition from research to industrialization.

One of the most important limitations to achieve the goal of a monolithic integrated photonic system is the indirect band gap nature of silicon, which impedes the availability of light sources in the complementary metal oxide semiconductor (CMOS) technology. Aside from the integrated light emitting device, most of the rest of the problems regarding Si photonics have been solved, being its lack virtually of the only thing separating us from making monolithic Si-based LOC technology.

Depending on the application, the light source problem can be tackled in different manners. In the specific case of biophotonic applications where visible light is preferred [1], the silicon-rich oxide (SRO) or off stoichiometric oxide can be used to obtain light emitting capacitors (LECs). The SRO-based LECs emit almost in all the visible light range, and they are totally silicon compatible [2]. In fact, the integration of a light source, waveguide, and a sensor has already been theoretically and experimentally demonstrated using standard CMOS technology [3, 4].

The active material in a LEC is a SRO film, which can be obtained implanting Si ions into thermally grown silicon dioxide or using a variety of chemical vapor deposition (CVD) techniques. One of the most popular of the latter is the low-pressure CVD (LPCVD), which is a simple way to produce SRO with different silicon excesses [5, 6]. SRO-LPCVD is characterized by the ratio R_0, defined as

$$R_0 = \frac{P_{N_2O}}{P_{SiH_4}} \tag{1}$$

where P_{N_2O} and P_{SiH_4} are the partial pressures of the nitrous oxide and silane gases, respectively. Under this equation, $R_0 = 3$ produces SRO films with 17% atomic silicon excess, while $R_0 > 100$ produces stoichiometric oxide. R_0 values between 20 and 30 produce SRO with silicon excess between 4 and 5 at.%, which delivers a luminescent material, but with relatively poor electrical conductivity. On the other hand, SRO with $R_0 = 10$ or less presents a lower light emission and higher conductivity than those of the former.

Aside from the SRO-based LECs, there are very few reports on totally Si-compatible integrated photonic circuits, most of which use reverse biased PN junctions as the light source [7–9]. Other proposed solutions include the use of phosphorus doped germanium heterojunctions [10], the coupling to the photonic circuit of optical fibers pig-tailed to lasers [11], or the hybrid approximation, in which external nonsilicon sources such as III–V reflective semiconductor optical amplifiers (RSOAs) are used [12]. All the previous lack the possibility of taking advantage of the current techniques used for the massive production of silicon-integrated circuits (ICs). Finally, another approach uses the implantation of rare-earth elements into silicon oxide to produce light emission in the infrared communication region [13]. Again, such technique is not compatible with the standard silicon IC technology.

Then, SRO-based LECs present themselves as the most promising solution to a fully IC-compatible integrated photonic circuit including the three basic elements, i.e., emitter, waveguide, and detector, as demonstrated in [4]. However, at this point, they work in the edge of electric breakdown and consume larger power than that needed to comply with IC strict standards. Therefore, SRO-based LECs require new strategies or different approaches to improve their performance.

In this work, we review the fabrication and performance of LECs, fabricated by our research group, that use different substrate treatments and a variety of SRO compositions and configurations, as means of discussing the strategies to improve the behavior of these devices.

2. Experimental procedure

SRO-based LECs were fabricated using different structures and conditions, namely, SRO monolayers on polished Si-wafers, SRO monolayers on textured Si substrates, and SRO multilayers (MLs) with gradual and abrupt silicon excess. For reference, LECs with single SRO films and SRO in a multilayered structure will be labeled as S-LEC and M-LEC, respectively. The standard fabrication process used is completely compatible with the CMOS technology. For textured Si substrates, the reactive ion etching (RIE) process was used. In this process, Ar and SF_6 in proportion of 7:3 and power of 300 W were set to roughening surface during 1 min, resulting in conical structures over the surface with a roughness and peak density of 4.0 ± 0.2 nm and 3.7×10^{10} cm^{-2}, respectively.

SRO films (mono- or multilayers) were deposited at 720°C, on N-type or P-type silicon substrates ((100)-oriented) with low resistivity (between 1 and 10 Ω × cm) by LPCVD and using the flow ratio (R_0) between N_2O and SiH_4 to vary the silicon excess. R_0 values of 5, 10, 20, 25, and 30 have been used to obtain different silicon excesses. Subscript of SRO labels indicates the R_0 parameter. After deposition, SRO films were thermally annealed at 1100°C for 3 h in nitrogen atmosphere in order to activate their photoluminescent (PL) emission.

For electrical and electroluminescent studies, metal insulator semiconductor (MIS)-like devices were fabricated. A semitransparent n^+ polycrystalline silicon (poly) gate was deposited onto the SRO film by LPCVD. After a photolithography process step, different shaped gates were defined. The backside contacts were obtained by the evaporation of an aluminum layer with thicknesses between 0.6 and 1 μm. Finally, the devices were thermally annealed at 480°C in forming gas in order to assure ohmic contacts.

The thickness of all samples, including multilayer structures, was measured using a null Gaertner L117 null ellipsometer with a He-Ne laser of 632.8 nm wavelength. PL spectra were obtained using a Horiba Yvon Fluoromax-3 spectrometer at room temperature; all the films were excited with UV radiation. Optical filters were used in order to guarantee the wavelength of the excitation beam. For electrical and electroluminescent studies, a source meter Keithley model 2400 was used. Electroluminescence (EL) spectra were obtained by biasing the devices with a constant DC voltage and measuring the emitted light by means of

an optical fiber normally aligned to the poly gate surface and connected to the Fluoromax 3 spectrometer. The optical power from the emitted light was measured with a 1400 IL radiometer connected to an UV-VIS GaAsP detector placed in front of the gate. Images from EL were obtained using a digital photographic camera. More specific details of the different characteristics of the studied LECs are addressed in Sections 3.1–3.3.

3. Results and discussion

3.1. SRO monolayers

This section shows the electro-optical properties of SRO films deposited on N-type silicon substrates using R_0 values of 20 (SRO_{20}) and 30 (SRO_{30}) and thicknesses of 70.1 ± 2.3 and 119.3 ± 4.9 nm, respectively. LECs with square-shaped poly gates of 4 mm^2 area and 400 nm thick were defined. To obtain PL spectra, the SRO samples (without poly gate) were excited using a 290 nm radiation.

The R_0 parameter is determinant in the structural, compositional, electrical, and light emitting characteristics of the SRO [14]. Red and blue electroluminescent devices have been obtained using R_0 = 20 and 30, respectively. **Figure 1** shows PL and EL spectra of S-LEC_{20} and S-LEC_{30}. There, it is possible to see that both samples emit red PL, but changes in the emission wavelength are obtained with electrical stimulation, especially for SRO_{30}, where a blue EL band is observed with the main peak at 468 nm. A long spectral shift, blue shift, of almost ~227 nm is observed between the EL and PL bands of the SRO_{30} films (blue dash line). LECs with SRO_{20} films emit a broad EL spectrum in the red region (713 nm), as observed in **Figure 1**. An additional EL peak of low intensity is also observed at 468 nm. There exists also a blue spectral shift of the EL with respect to the PL spectrum in SRO_{20} films but much smaller, remaining in the red side of the spectrum (red dash line), which could indicate that the same luminescent centers are involved in both luminescence types. In both SROs, the EL emission is bright and

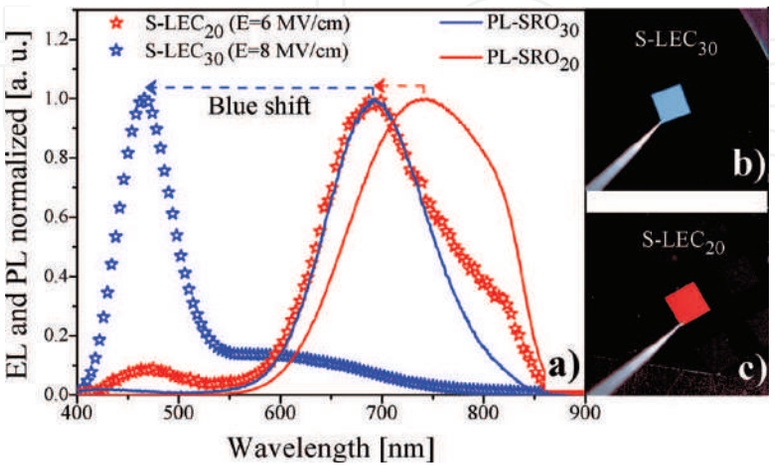

Figure 1. (a) PL (solid line) and EL (symbols) spectra of S-LEC_{20} and S-LEC_{30}. Images of (b) blue (S-LEC_{30}) and (c) red (S-LEC_{20}) bright emission.

observable to the naked eye, as shown in **Figure 1(b)** and **(c)**. Notably, this intense EL is emitted in the whole area of the LEC devices. As expected, the intensity of the full-area emission increases as the applied electric field is increased [15].

Different authors have attributed the spectral shift between PL and EL to three different origins: defects in the SiO_2 matrix, band filling when bipolar injection is achieved, and silicon nanocrystal (Si-nc) size selection by the injected electrons energy [16–18]. In our case, the red EL observed in S-LEC_{20} is ascribed to surface defects on the Si-ncs, which have been observed by transmission electron microscopy (TEM) [14]. While the blue EL in SRO_{30} devices is consistent with the emission related to defects such as oxygen defect centers (ODC), non-bridging oxygen hole centers (NBOHC), and E'_δ centers, which can be either intrinsically present or generated by the electrical stress applied to the SRO matrix [14].

Regarding the electrical behavior, two different electrical behaviors have been obtained from the red and blue LECs. **Figure 2** shows the current density (J) as a function of the electric field (E) of LECs working in accumulation mode (positive bias to the gate).

The S-LEC_{30} shows a high current state (HCS) at low electric fields (<4 MV/cm), followed by a switch by the current to a low conduction state (LCS). Our group has observed this resistive switching (RS) from the HCS to LCS in previous studies and at both forward and reverse biases [14, 15, 19–21]. Such effect was related to the annihilation of conductive paths created by adjacent stable silicon nanoparticles (Si-nps) and unstable silicon nanoclusters (Si-ncls) in which Si-Si bonds can be broken creating some structural changes (defects), including some blue luminescent centers [15, 19, 20]. Recent reports regarding the same electrical switching in SRO films were observed, relating it to the presence of a conductive nanofilament [21–24]. Analysis of TEM imaging showed that the filament is created and annihilated by structural changes due to Joule heating effect produced by the high current flow, which allows the

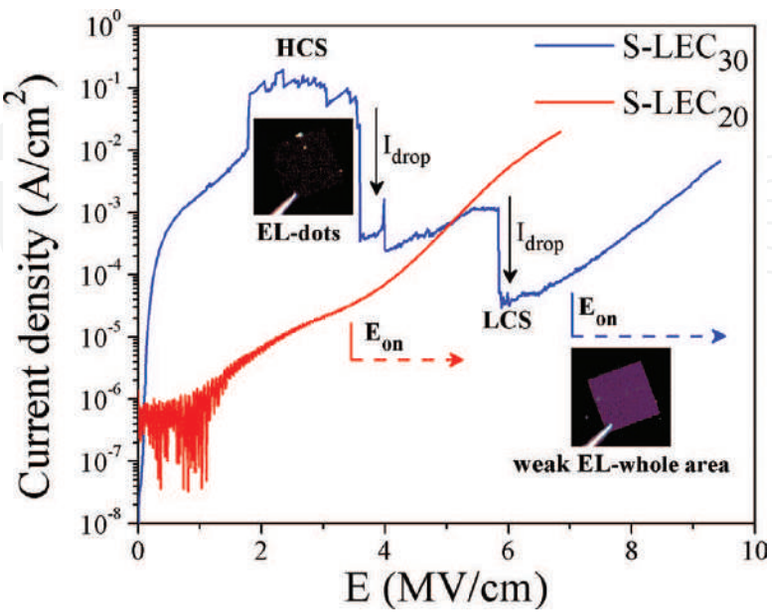

Figure 2. J-E curve from SRO_{30}- and SRO_{20}-based LECs. Insets are depicting images of EL dots and weak whole area EL.

crystallization (HCS) or amorphization (LCS) of the nanofilament [25]. These observations agree with our asseverations regarding the resistive switching observed in our S-LEC$_{30}$ [24]. During HCS regime, current jumps and drops corresponding to the appearance or disappearance of electroluminescent spots (EL dots) on the LEC surface have been observed (see inset in **Figure 3**) [14, 15, 19, 20]. Once the current fluctuations disappear, through an electrical annealing, the current behavior stabilizes allowing for the whole area EL [2, 14, 19].

On the other hand, the electrical behavior of most of LECs with SRO$_{20}$ films does not show current fluctuations. This effect has been related to the presence of well-separated Si-ncs and observed mainly on samples with a relatively high density of Si-nps [14]. This suggests that a denser network of conductive paths becomes more likely as the Si-ncs density increases, allowing for a uniform charge flow through the whole capacitor area.

In fact, it has been found that the trap-assisted tunneling (TAT) conduction mechanism, through a quasi-continuum of defect traps, predominates in the HCS in the S-LEC$_{30}$ devices, where the trap energy (ϕt) was estimated to be around 1.99 eV [14]. The TAT conduction mechanism has been reported in SRO-based devices where the RS phenomenon has been observed, in agreement with the observation of the devices reported in this work [24]. On the other hand, Poole-Frenkel (P-F) tunneling was found to be the most likely charge transport mechanism in the S-LEC$_{20}$ devices.

Although excellent results have been obtained from light emitting devices based on SRO with Ro = 20 and 30, the turn-on electric field (E$_{on}$) is still higher than desired. As an improvement strategy to obtain devices that emit in a wider range of wavelengths, and at lower E$_{on}$, multilayer structures involving SRO$_{10}$, SRO$_{20}$, and SRO$_{30}$ layers have been designed and fabricated. As it has been shown, both SRO$_{20}$ and SRO$_{30}$ exhibit intense PL. On the other hand, SRO films with higher R$_0$ show lower PL intensity but better conductive characteristics [15, 26]. If the characteristics of each SRO film are preserved in a SRO ML structure, it is possible to improve the charge injection and luminescence properties of SRO-based LECs using the band-gap engineering by the Si-nc size modulation. Under this approach, the composition, structural,

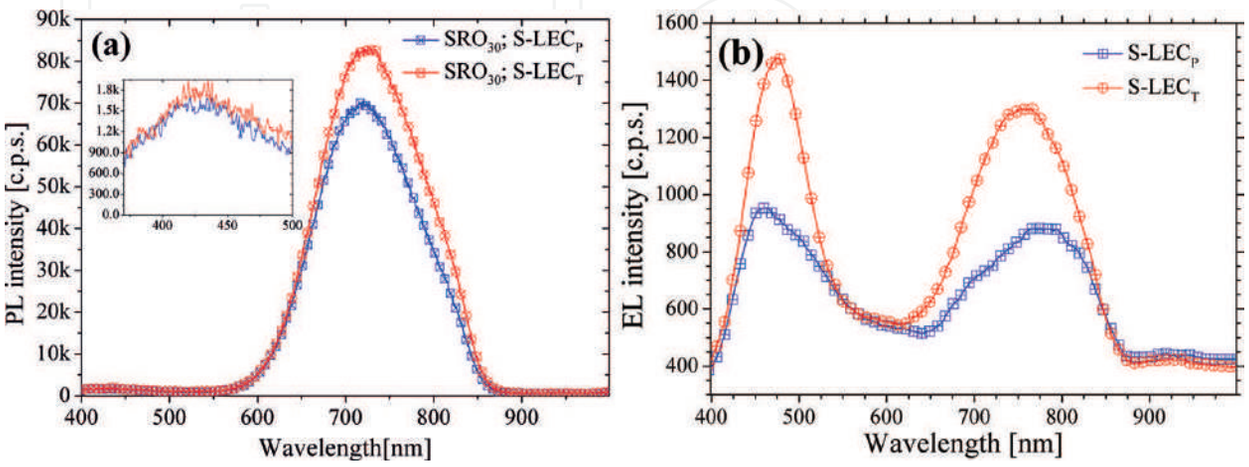

Figure 3. (a) PL spectra from SRO$_{30}$ films of S-LEC$_P$ and S-LEC$_T$. SRO films were excited with λ = 300 nm. (b) EL spectra for S-LEC$_P$ and S-LEC$_T$, when LECs were electrical polarized with 11.5 and 9.8 MV/cm.

and PL emission characteristics of SRO MLs with gradual change of R_0 from 10 to 30, and conversely, have been studied [27]. The Si and O gradual composition profiles in the $SRO_{10–20-30}$ multilayered system have been confirmed by X-ray photoelectron spectroscopy (XPS). The PL emission in these gradual SRO MLs increases when the emissive SRO layers (Ro = 20 and 30) are in the center of the ML. Moreover, the gradual Si-nc size according to the R_0 of each layer was preserved. Nevertheless, the study of the electro-optical characteristics of LECs with such scheme is still being carried out.

3.2. SRO monolayers on textured substrates

To evaluate the performance improvement of LECs on textured substrates (labeled as $S\text{-}LEC_T$), a SRO_{30} film with thickness of about 70 nm was used. The textured process was described in the experimental section. The SRO_{30} film was also deposited on a regular polished substrate, as a reference device, labeled as $S\text{-}LEC_{P.}$ In both cases, the substrate was a P-type silicon wafer with resistivity between 2 and 4 Ω × cm. Over the SRO, a 250-nm thick square gate of poly layer with an area of 1.54 mm^2 was deposited and defined. **Table 1** summarizes characteristics of both S-LECs.

Figure 3(a) shows the PL spectra of the SRO_{30} film present in the S-LECs. Roughening does not appear to significantly affect the emission properties of the active material when it is optically stimulated, as previously demonstrated [28, 29]. As can be observed, there are two peaks, one centered at 725 nm (red band) and a much weaker one at 428 nm (blue band, shown in the inset of **Figure 3(a)**). The emission in blue band is ascribed to non-bridging oxygen defects and oxygen deficiency-related centers [14, 30–34], whereas the red band is attributed to oxygen vacancies caused by the Si excess (720 to 740 nm) [31–33], as well as to interfacial defects in boundaries of silicon nanoclusters with the silicon oxide matrix (810 nm) [35–37].

Figure 3(b) exhibits the EL spectra of the S-LECs. Both LECs show two bands as well: blue and red, as PL. This indicates that PL and EL have the same origin, mainly attributed to SRO-related defects [25, 34, 37]. Since in this case the samples are electrically pumped, electrons are driven through deeper traps, allowing for a larger amount of radiative transitions of higher energy, such that emission in the blue band has comparable intensities to those of the red one. This phenomenon is not observed in PL due to its lower energetic source (UV radiation). $S\text{-}LEC_T$ reached a higher EL intensity than $S\text{-}LEC_P$. Additionally, $S\text{-}LEC_T$ requires less electrical power than $S\text{-}LEC_P$ to achieve its maximum intensity.

Figure 4 displays the J vs. E curve for both textured and non-textured LECs. The J-E curve exhibits the behavior of S-LECs for positive voltage, condition in which EL is observed. Under

ID	Texturing	Roughness [nm]	Peak density [cm^{-2}]	SRO_{30} thickness [nm]
$S\text{-}LEC_P$	No	0.5	0	65.9 ± 0.4
$S\text{-}LEC_T$	Yes	4.0 ± 0.2	$3.7 \pm 1.8 \times 10^{10}$	68.8 ± 1.7

Table 1. Roughening features and SRO_{30} thickness of $S\text{-}LEC_P$ and $S\text{-}LEC_T$.

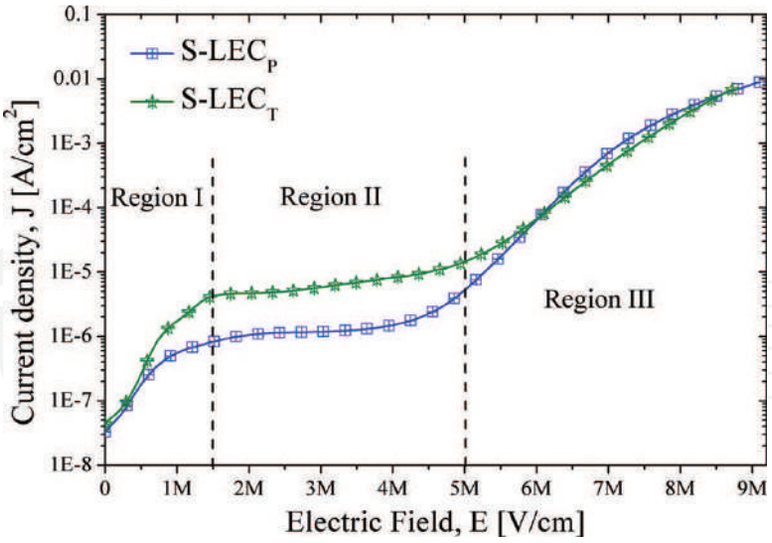

Figure 4. Current density as a function of electric field of S-LECs. Curves are divided in three regions, according to the conduction mechanism for each E range.

this condition, an inversion layer is formed in the SRO/Si-substrate interface. S-LECs presented in this section did not show current jumps, neither the RS from HCS to a LCS, contrary to other reports [14, 15, 19–24]. At low electric fields (region I), the ohmic conduction mechanism dominates the carrier transport; however, roughening of the substrate surface in S-LEC$_T$ propitiates a current increase due to the conical structures in silicon surface, which act as tips highly populated by electrons allowing for higher injection rates through the SRO layer. At medium electric fields (region II), the Fowler-Nordheim tunneling mechanism is responsible for the conduction. In this regimen, the observed current offset between curves of S-LECs is due to the augment of current density at lower electric fields; however, both curves present comparable slope [28]. At the higher electric fields (region III), the trap-assisted tunneling mechanism controls the carrier transport. In this regimen, both S-LEC$_P$ and S-LEC$_T$ present electroluminescence, in agreement with results of the LECs presented in Section 3.1. As can be seen in **Figure 4**, in region III the J-E curves of S-LECs overlap, but even though they have similar electrical responses, S-LEC$_T$ achieves a substantial improvement of electro-optical properties as compared to its counterpart, as it will be shown later.

3.3. SRO multilayers

LECs based on multilayered structures are obtained by a multistep deposition process. While the samples remain in the reactor, the LPCVD system is periodically adjusted to change the R_0, modifying the silicon excess in the layer deposited during each period. Two structures were fabricated: M-LEC$_{525}$ and M-LEC$_{1025}$, which alternate four mainly conductive layers ($R_0 = 5$) with three primarily emitting layers ($R_0 = 25$). For both devices, P-type silicon wafers with resistivity between 2 and 4 Ω × cm were used as substrate.

M-LEC$_{525}$ has SRO$_5$ as conductive layer and SRO$_{25}$ as emitting layer, with thickness of 15 and 25 nm, respectively. Meanwhile, M-LEC$_{1025}$ uses the same material for emitting layers but

SRO_{10} instead of SRO_5, with thickness of 10 nm. The nominal thickness of the whole structure is 115 nm approximately. In the top of the multilayer, a semitransparent 250 -nm thick n^+ polycrystalline silicon layer was deposited, and a square gate with an area of 4.05 mm^2 was formed.

Figure 5(a) shows the PL spectra of the SRO multilayers. Two bands are observed: blue and red bands. The shape of PL spectra is quite similar to that of SRO_{30}, which does not have Si-ncs [25], suggesting that, as in SRO_{30}, oxygen defects in the oxide matrix due to the silicon excess are the main cause of PL emission in multilayered structures [34]. As it is reported in [37], Si-ncs are observed in SRO multilayers, and their size and density depend on the features of each layer (silicon excess, thickness, etc.), in agreement with other reports on multilayers [27, 34, 38]. **Table 2** summarizes the Si-nc features of M-LECs. **Figure 5(b)** and **(c)** displays the EL spectra of M-LECs. Again, two luminescent bands are obtained; however, $M\text{-}LEC_{525}$ has a more prominent blue band, whereas $M\text{-}LEC_{1025}$ achieves higher emission in red band. In [37], this difference is associated with the size and density of Si-ncs embedded in the conductive layers. In $M\text{-}LEC_{525}$, SRO_5 layers allow electrons reach deeper traps (blue emission centers); meanwhile $M\text{-}LEC_{1025}$ requires higher electric fields (energy) in order to excite the same emission centers. Thus, conductive layers with bigger size and lower density of Si-ncs produce

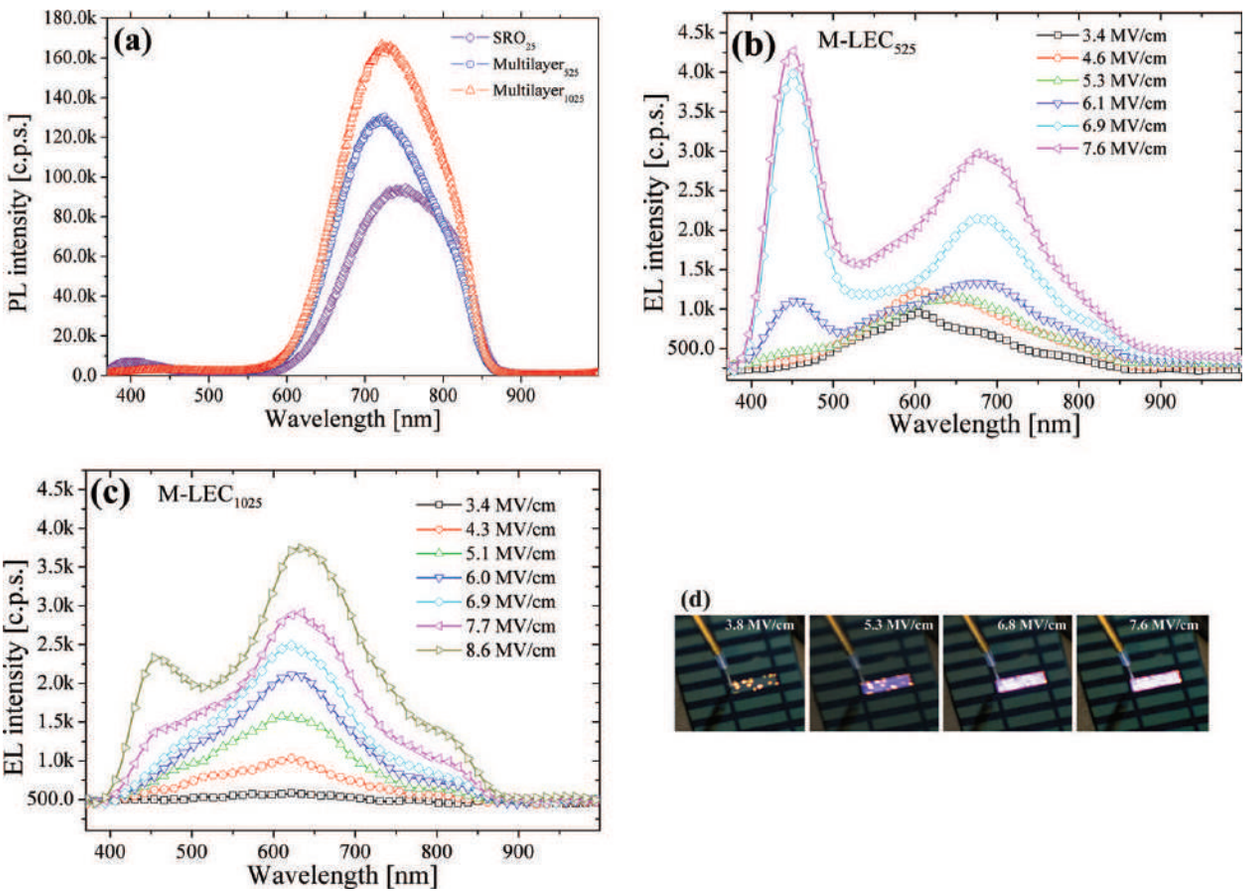

Figure 5. (a) PL spectra of SRO multilayers of M-LECs. SRO mono- and multilayers were excited with λ = 300 nm. EL spectra of (b) $M\text{-}LEC_{525}$ and (c) $M\text{-}LEC_{1025}$. (d) EL emission of $M\text{-}LEC_{525}$ for different electric fields. Note that whole area emission and localized bright spots can coexist.

ID	Si-nc size of CL* [nm]	Si-nc density in CL [cm³]	Si-nc size of EmL** [nm]	Si-nc density in EmL [cm³]	Nominal thickness [nm]
M-LEC$_{525}$	4.0	1.06×10^{12}	2.1	5.76×10^{11}	131.1 ± 7.6
M-LEC$_{1025}$	3.6	1.30×10^{12}	1.8	7.43×10^{11}	116.7 ± 1.6

*CL—conductive layer.
**EmL—emitting layer.

Table 2. Size and density of Si-nc in each layer, as well as nominal thickness of multilayered structure.

M-LECs with brightest blue emission at lower electric fields. **Figure 5(d)** shows digital pictures of the EL emission of M-LEC$_{525}$ biased with different electric fields, where blue color is predominant in the emission.

Figure 6 exhibits J-E characteristics of the M-LECs. In a first test, M-LECs present a LCS, but once they reach a high electric field (E > 5 MV/cm), M-LECs change to a HCS and remain in this regimen for the subsequent measurements, as previously reported in [39] and agreeing with others works [34, 40]. During first current-voltage measurement, Si-ncs are ordered forming conductive trajectories (electroforming) whereby electrons can be easily driven through the SRO multilayers [22, 23]. Across their conductive path, they can impact other electrons not only increasing the current density but also augmenting the number of electrons able to decay at different trap levels, enhancing the emission intensity as well. In [39], it is reported that thermionic emission, Poole-Frenkel, trap-assisted tunneling, and impact ionization conduction mechanisms are responsible for the charge transport. The first two dominate conduction in low (E < 2 MV/cm) and medium (2 MV/cm < E < 4 MV/cm) electric field regimes, respectively. Meanwhile, TAT and impact ionization are responsible for charge transport in

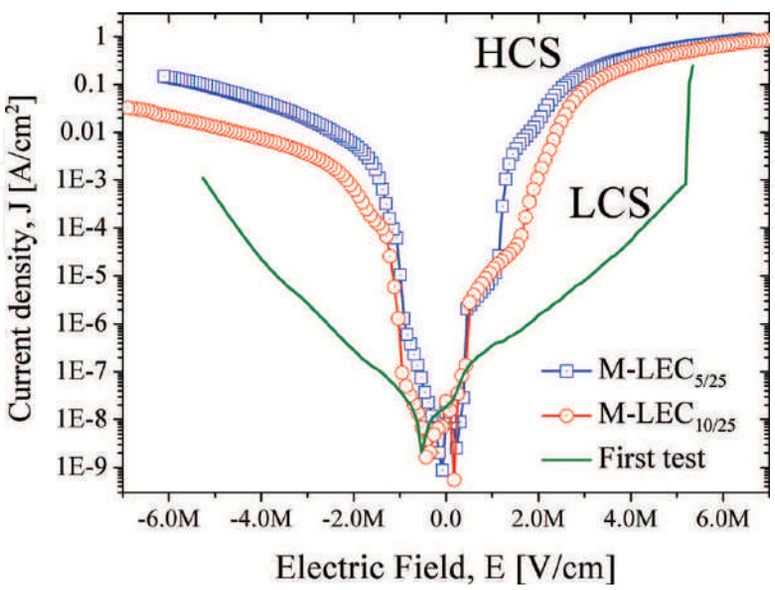

Figure 6. Current density as a function of electric field for M-LECs. In a first sweep, M-LECs present a LCS, but once they achieve a HCS, LECs preserve this behavior maintaining EL emission.

high-energy regime, which is also the region where brightest EL is observed. For E < 6 MV/cm, only TAT mechanism is presented, but once electric field overpass 6 MV/cm, impact ionization takes place, increasing substantially the EL intensity.

4. Discussion

Figure 7(a) and **(b)** shows, respectively, the normalized PL spectra and the J-E curve for S-LEC$_P$, S-LEC$_T$, M-LEC$_{525}$, and M-LEC$_{1025}$ in order to compare single- and multilayer-based LECs. Regarding PL response, multilayer of M-LEC$_{1025}$ records the highest intensity, followed by M-LEC$_{525}$ and single SRO$_{25}$ and SRO$_{30}$ layers. The total PL emission in a multilayered structure has two contributions: emission of SRO$_{25}$ layers, which is the main contribution, and emission from the conductive SRO layers (SRO$_5$ or SRO$_{10}$), which have a smaller contribution [37]. As reported in [26], SRO films with higher density of Si-ncs with size lower than 3 nm have the brighter emission. In these films, defects are formed at the interface between SRO and the Si-ncs, acting as localized states from where electrons decay through ground states, emitting light in the process. Even though conductive SRO layers mainly enhance electrical characteristics in M-LECs, the presence of Si-ncs into SiO$_x$ matrix propitiates a non-negligible contribution to PL emission, and as can be observed in **Table 2**, the highest density with the lowest size of Si-ncs is achieved in M-LEC$_{1025}$, in agreement with PL response.

In **Figure 7(b)**, J-E curves of LECs are presented. A substantial augment of current density in M-LECs with respect to that one in S-LECs can be observed. M-LECs reach the HCS at lower voltages. This improvement of carrier transport in M-LECs is ascribed to the high silicon content in SRO conductive layers. In the electroforming process observed in these M-LECs, which occurs in the first J-E measurement, Si-ncs are connected creating multiple preferential conductive paths between the poly and Si-substrate. Electrons can easily flow through those conductive trajectories in SRO MLs improving the current density. Regarding S-LECs, SRO layer does not have Si-ncs to form conductive paths; however, it has a high density of defects.

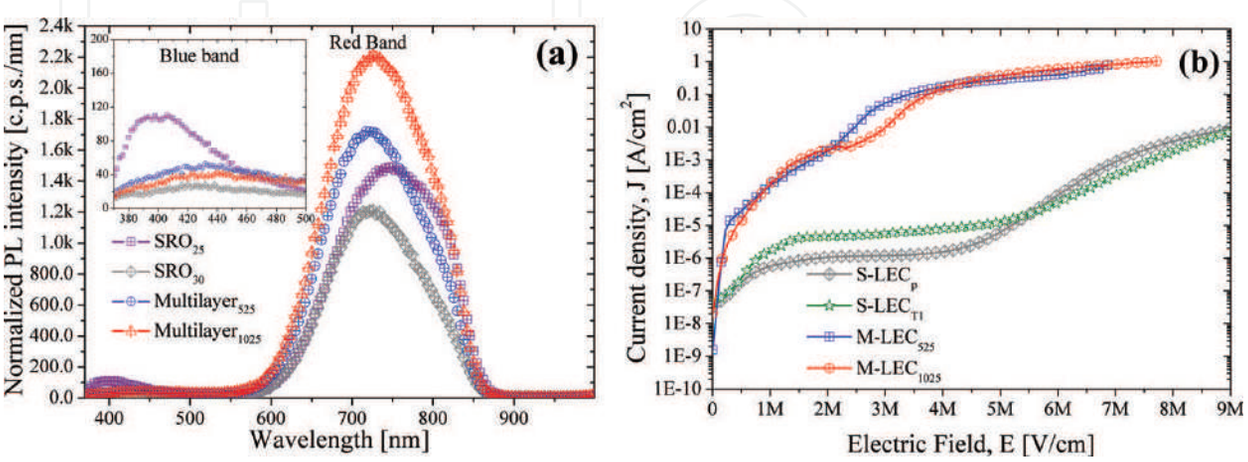

Figure 7. (a) PL spectra normalized with respect to thickness of the SRO single or multilayer. (b) Current density as a function of electric field for S-LECs and M-LECs.

This high content of defects allows that electron transit by a sequence of low energetic traps through the SRO film, named as low resistive trajectories. Even though these trajectories are low resistive, the charge-trapping effect still takes place, such that enhancement of current density is limited and a HCS is not reached. Fabricating S-LECs on textured substrate allow improvement of carrier injection to the SRO film; however, this technique also has results with lower current density improvement than those in a multilayered structure.

Figure 8 displays the integrated EL intensity as a function of electric field for (a) S-LECs on polished substrates and (b) S-LECs on textured substrate and M-LECs. These figures allow comparing LECs by means of two figures of merit: turn-on electric field (E_{on}) and the operation range. The E_{on} is the electric field needed for the EL intensity to overpass the noise level and begin to rise; meanwhile, the operation range is the electric field range in which LECs emit light without electrical damage, and it must go from E_{on} to an E value before dielectric breakdown.

As it can be seen in **Figure 8(a)**, S-LEC_{20} (devices that emit in red) operate on a greater range (from 3.7 to 6 MV/cm) than S-LEC_{30} (devices that emit in blue), which works from 7.0 to 8.3 MV/cm, approximately. The electric field range where it was possible to register EL spectra for S-LEC_{30} is 7.1–8.3 MV/cm and for S-LEC_{20} is 3.7–5.7 MV/cm. As can be noted, a larger electric field is required to obtain the blue emission as compared to the red one. In accordance, the devices without Si-ncs into SRO films and emitting in blue wavelengths require a larger electric field (E > 7MV/cm) to turn on. Additionally, a nearly linear fitting was done to the experimental data. The slope found for each device is slightly different, suggesting that the mechanisms responsible of the EL increase are not the same. A quite similar conclusion was obtained in Section 3.1, where EL emission is observed when TAT and P-F mechanisms dominate the charge transport in S-LEC_{30} and S-LEC_{20}, respectively.

In **Figure 8(b)**, it is found that the operation range of S-LEC_P and S-LEC_T is from 8.5 to 11.5 MV/cm and from 7 to 10 MV/cm, respectively. These operation ranges are lower than that one of M-LECs, which have an operation range from 3 to 9 MV/cm, approximately. Thus, M-LECs

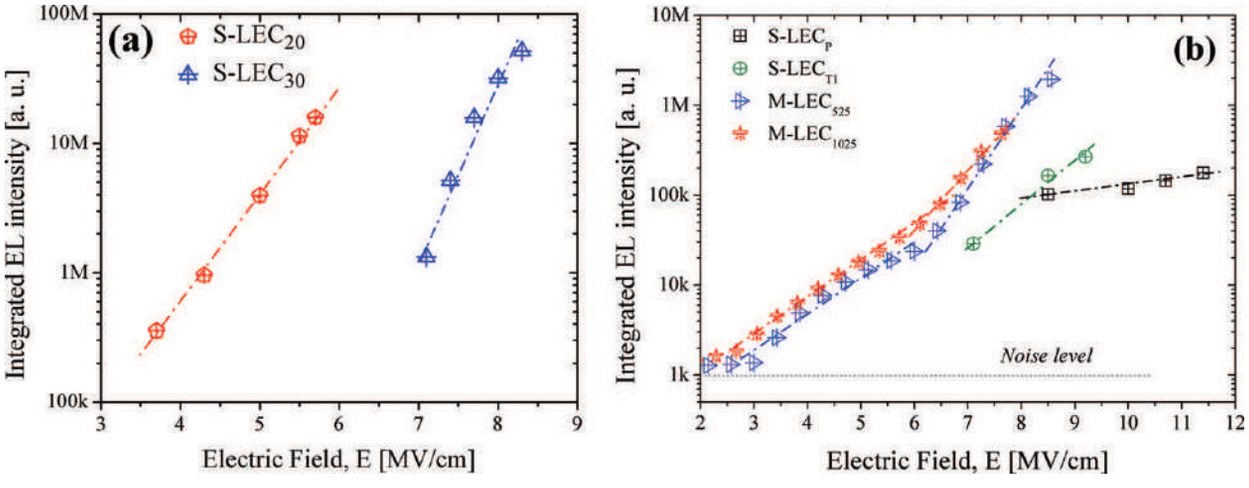

Figure 8. Integrated EL intensity as a function of electric field for (a) single-layer LECS and (b) single-layer LECs on textured substrate and M-LECs. Noise level is used as reference to evaluate EL emission of LECs. Intensities of graph (a) are not comparable with graph (b) because of differences in setup and testing condition.

ID	Voltage [V]	E [MV/cm]	Current [μA]	P_e [mW]	P_{opt} [μW]	η_c [10^{-4} %]
S-LEC_P	80	11.4	113	9.04	0.17	18.7
S-LEC_{T1}	68	9.7	78	5.30	0.34	64.1
M-LEC_{525}	95	7.3	30×10^3	2.85×10^3	2.75	1.0
M-LEC_{1025}	95	8.2	37×10^3	3.52×10^3	2.71	0.9

Table 3. Voltage, electric field, electrical power, optical power, and conversion efficiency of LECs: single layer, roughening substrate, and multilayers.

have twice higher operation range than S-LECs. Moreover, the E_{ON} value of M-LECs is lower than that one of S-LECs, and the EL intensity of M-LECs gradually increases as the electric field becomes stronger. In contrast, S-LECs require a higher electric field to emit light, and their transition from turn-off state to turn-on state is abrupt. Hence, M-LECs are better candidates to be integrated in all-silicon photonic circuits due to the lower E_{on} and a wider operation range.

Finally, the conversion efficiency (η_c) is analyzed for each device. The η_c is defined as the ratio of the optical power (P_{opt}) with respect to the electrical power (P_e). The latter power is calculated as $P_e = V*I$, where V is the voltage and I is the electrical current in which a specific P_{opt} is measured. **Table 3** resumes values of voltage, electrical current, P_e, P_{opt}, and conversion efficiency (η_c) of LECs with the different strategies used. These parameters were selected considering the best electro-optical performance. As we can see, the S-LECs are more efficient but have lower values of P_{opt}, while M-LECs are less efficient but achieve a significantly higher P_{opt}. Based only on efficiency and without considering the application, S-LECs would be the best option; however, as is aforementioned, M-LECs have other advantages over S-LECs. A higher operation range, lower E_{on} values, an EL intensity that gradually increases, and a greater P_{opt} are the features that place M-LECs as the best option to be integrated in all-silicon photonic circuit. In [4], it has been demonstrated that S-LECs are enough to guaranty the functionality of all-silicon photonic circuits; however, the LECs operate close to the noise level. Thus, the performance of such system could be improved using M-LECs, which have enhanced electro-optical characteristics.

5. Conclusion(s)

This work was focused on the different strategies used to improve the performance of SRO-based LECs fully compatible with the CMOS technology to be integrated in an all-silicon photonic circuit. We reviewed the fabrication and characterization of LECs that use different substrate treatments and a variety of SRO compositions and configurations. LECs were fabricated with single SRO layers (S-LECs) deposited on polished and textured Si substrates. LECs with SRO in a multilayered structure (M-LECs) involving a conductive SRO layer with an emitting one were also fabricated.

It was found that M-LEC_{1025} emits the highest PL intensity, followed by M-LEC_{525} and finally those with single SRO_{25} and SRO_{30} layers. An improved charge injection observed through

an augment of current density was obtained in M-LECs with respect to S-LECs, even though S-LECs use textured silicon substrate to improve carrier injection. M-LECs achieve high conduction state with lower voltages, which is ascribed to the high silicon content in SRO conductive layers, forming conductive trajectories by means of electrons that are easily driven through multilayers.

The electro-optical characterization of different LECs exhibited that M-LECs have twice higher operation range than S-LECs. Moreover, M-LECs emit at lower electric fields and their intensity gradually increases as the electric field becomes stronger. In the opposite, S-LECs require a high electric field to emit light, and their transition from turn-off state to turn-on state is abrupt. Hence, M-LECs perform a better behavior to be integrated in all-silicon photonic circuits based on a lower E_{on} and wider operation range. A higher operation range, lower E_{on}, EL emission that gradually increase, and a greater P_{opt} are the features that place M-LEC as the best option to be integrated in all-silicon photonic circuit.

Acknowledgements

Authors want to thank the financial support from CONACYT. L Palacios-Huerta and A.A. González-Fernández acknowledge CONACYT for the postdoctoral grant. The help of technicians Pablo Alarcon, Victor Aca, and Armando Hernández is also appreciated.

Conflict of interest

Authors declare that there is no conflict of interest.

Author details

Jesús Alarcón-Salazar[1], Liliana Palacios-Huerta[1], Alfredo Abelardo González-Fernández[1], Alfredo Morales-Sánchez[2]* and Mariano Aceves-Mijares[1]*

*Address all correspondence to: alfredo.morales@cimav.edu.mx and maceves@inaoep.mx

1 Electronics Department, National Institute of Astrophysics Optics and Electronics, Tonantzintla, Puebla, Mexico

2 Advanced Materials Research Center (CIMAV), Monterrey-PIIT, Apodaca, Nuevo Leon, Mexico

References

[1] Muñoz P, Micó G, Bru L, Pastor D, Pérez D, Doménech J, Fernández J, Baños R, Gargallo B, Alemany R, Sánchez A, Cirera J, Mas R, Domínguez C. Silicon nitride photonic

integration platforms for visible, near-infrared and mid-infrared applications. Sensors. 2017;**17**(9):2088. DOI: 10.3390/s17092088

[2] Fernández AAG, Mijares MA, Sánchez AM, Leyva KM. Intense whole area electroluminescence from low pressure chemical vapor deposition-silicon-rich oxide based light emitting capacitors. Journal of Applied Physics. 2010;**108**(4):43105. DOI: https://doi.org/10.1063/1.3465335

[3] Alarcón-Salazar J, Zaldívar-Huerta IE, Aceves-Mijares M. An optoelectronic circuit with a light source, an optical waveguide and a sensor all on silicon: Results and analysis of a novel system. Optics & Laser Technology. 2016;**84**:40-47. DOI: https://doi.org/10.1016/j.optlastec.2016.04.013

[4] González-Fernández AA, Juvert J, Aceves-Mijares M, Domínguez C. Monolithic integration of a silicon-based photonic transceiver in a CMOS process. IEEE Photonics Journal. 2016;**8**(1):1-13. DOI: 10.1109/JPHOT.2015.2505144

[5] Dong DRYD, Irene EA. Preparation and some preparation and some properties of chemically vapor-deposited Si-rich SiO and SigN, films D. Journal of the Electrochemical Society (JES) and the ECS Journal of Solid State Science and Technology. 1977;**5**:819-823. DOI: doi: 10.1149/1.2131555

[6] Alarcón-Salazar J, López-Estopier R, Quiroga-González E, Morales-Sánchez A, Pedraza-Chávez J, Zaldívar-Huerta IE, Aceves-Mijares M. Silicon-Rich oxide obtained by low-pressure chemical vapor deposition to develop silicon light sources. In: Sudheer Neralla, editor. Chemical Vapor Deposition - Recent Advances and Applications in Optical, Solar Cells and Solid State Devices. InTech; 2016. DOI: 10.5772/63012. http://dx.doi.org/10.5772/63012

[7] Ogudo KA, Schmieder D, Foty D, Snyman LW. Optical propagation and refraction in silicon complementary metal-oxide-semiconductor structures at 750 nm: Toward on-chip optical links and microphotonic systems. Journal of Micro/Nanolithography, MEMS, and MOEMSournal of Micro/Nanolithography, MEMS, and MOEMS. 2013;**12**(1):13015. DOI: 10.1117/1.JMM.12.1.013015

[8] Xu K, Ning N, Ogudo KA, Polleux J-L, Yu Q, Snyman LW, Light emission in silicon: From device physics to applications. In: Proceedings of the SPIE 9667, International Workshop on Thin Films for Electronics, Electro-Optics, Energy, and Sensors. 2015:966702-1-966702-10. https://doi.org/10.1117/12.2199841

[9] Misiakos K, Petrou PS, Kakabakos SE, Yannoukakos D, Contopanagos H, Knoll T, Nounesis G. Fully integrated monolithic optoelectronic transducer for real-time protein and DNA detection: The NEMOSLAB approach. Biosensors and Bioelectronics. 2010;**26**(4):1528-1535. DOI: https://doi.org/10.1016/j.bios.2010.07.104

[10] Camacho-Aguilera RE, Cai Y, Patel N, Bessette JT, Romagnoli M, Kimerling LC, Michel J. An electrically pumped germanium laser. Optics Express. 2012;**20**(10):11316. DOI: https://doi.org/10.1364/OE.20.011316

[11] Sun C, Wade MT, Lee Y, Orcutt JS, Alloatti L, Georgas MS, Waterman AS, Shainline JM, Avizienis RR, Lin S, Moss BR, Kumar R, Pavanello F, Atabaki AH, Cook HM, Ou AJ, Leu JC,

Chen Y-H, Asanović K, Ram RJ, Popović MA, and Stojanović VM. Single-chip microprocessor that communicates directly using light. Nature. 2015;**528**(7583):534-538. DOI: https://doi.org/10.1038/nature16454

[12] Gonzalez-Fernandez AA, Liles AA, Persheyev S, Debnath K, O'Faolain L. Wavelength-controlled external-cavity laser with a silicon photonic crystal resonant reflector. In: Schröder H, Chen RT, editors. Proc. SPIE 9753, Optical Interconnects XVI, San Francisco, California. 2016. pp. 975317. DOI: https://doi.org/10.1117/12.2213288

[13] Jambois O, Berencen Y, Hijazi K, Wojdak M, Kenyon AJ, Gourbilleau F, Rizk R, Garrido B. Current transport and electroluminescence mechanisms in thin SiO2 films containing Si nanocluster-sensitized erbium ions. Journal of Applied Physics. 2009;**106**(6):063526-063532. DOI: https://doi.org/10.1063/1.3213386

[14] Palacios Huerta L, Cabañas Tay SA, Luna López J-A, Aceves M, Coyopol A, Morales-Sánchez A. Effect of the structure on luminescent characteristics of SRO-based light emitting capacitors. Nanotechnology. 2015;**26**(39):395202. DOI: https://doi.org/10.1088/0957-4484/26/39/395202

[15] Morales-Sánchez A, Monfil-Leyva K, González AA, Aceves-Mijares M, Carrillo J, Luna-López JA, Domínguez C, Barreto J, Flores-Gracia FJ. Strong blue and red luminescence in silicon nanoparticles based light emitting capacitors. Applied Physics Letters. 2011; **99**:171102. DOI: https://doi.org/10.1063/1.3655997

[16] Lai BH, Cheng CH, Lin GR. Electroluminescent wavelength shift of Si-rich SiOx based blue and green MOSLEDs induced by O/Si composition Si-QD size variations. Optical Materials Express. 2013;**3**(2):166. DOI: https://doi.org/10.1364/OME.3.000166

[17] Wang DC, Chen JR, Zhu J, Lu C-T, Lu M. On the spectral difference between electroluminescence and photoluminescence of Si nanocrystals: A mechanism study of electroluminescence. Journal of Nanoparticle Research. 2013;**15**(11):2063. DOI: https://doi.org/10.1007/s11051-013-2063-x

[18] Chen D, Xie ZQ, Wu Q, Zhao YY, Lu M. Electroluminescence of Si nanocrystals-doped SiO_2. Chinese Physics Letters. 2007;**24**(8):2390. DOI: https://doi.org/10.1088/0256-307X/24/8/064

[19] Morales-Sánchez A, Barreto J, Domínguez C, Aceves M, Luna-López JA. The mechanism of electrical annihilation of conductive paths and charge trapping in silico- rich oxides. Nanotechnology. 2009;**20**(4):045201. DOI: https://doi.org/10.1088/0957-4484/20/4/045201

[20] Morales-Sánchez A, Barreto J, Domínguez C, Aceves-Mijares M, Luna-López JA, Perálvarez M, Garrido B. DC and AC electroluminescence in silicon nanoparticles embedded in silicon-rich oxide films. Nanotechnology. 2010;**21**(8):085710. DOI: https://doi.org/10.1088/0957-4484/21/8/085710

[21] Yao J, Sun Z, Zhong L, Natelson D, Tour JM. Resistive switches and memories from silicon oxide. Nano Letters. 2010;**10**(10):4105. DOI: 10.1021/nl102255r

[22] Yao J, Zhong L, Natelson D, Tour JM. In situ imaging of the conducting filament in a silicon oxide resistive switch. Scientific Reports. 2012;**2**(242):1-5. DOI: 10.1038/srep00242

[23] Mehonic A, Vrajitoarea A, Cueff S, Hudziak S, Howe H, Labbé C, Rizk R, Pepper M, Kenyon AJ. Quantum conductance in silicon oxide resistive memory devices. Scientific Reports. 2013;**3**:2708. DOI: 10.1038/srep02708

[24] Mehonic A, Cueff S, Wojdak M, Hudziak S, Labbé C, Rizk R, Kenyon A. Electrically tailored resistance switching in silicon oxide. Nanotechnology. 2012;**23**(45):455201. DOI: https://doi.org/10.1088/0957-4484/23/45/455201

[25] Aceves-Mijares M, González-Fernández AA, López-Estopier R, Luna-López A, Berman-Mendoza D, Morales A, Falcony C, Domínguez C, Murphy-Arteaga R. On the origin of light emission in silicon rich oxide obtained by low-pressure chemical vapor deposition. Journal of Nanomaterials. 2012;**2012**:890701. DOI: http://dx.doi.org/10.1155/2012/890701

[26] Morales-Sánchez A, Barreto J, Domínguez-Horna C, AcevesMijares M, Luna López JA. Optical characterization of silicon rich oxide films. Sensors and Actuators A. 2008;**142**:12-18. DOI: https://doi.org/10.1016/j.sna.2007.03.008

[27] Palacios Huerta L, Cabañas-Tay SA, Cardona Castro MA, Aceves Mijares M, Domínguez Horna C, Morales Sánchez A. Structural and optical properties of silicon rich oxide films in graded-stoichiometric multilayers for optoelectronic devices. Applied Physics Letters. 2016;**109**:031906. DOI: https://doi.org/10.1063/1.4959080

[28] Alarcón-Salazar J, Vásquez-Agustín MA, Quiroga-González E, Zaldívar-Huerta IE, Aceves-Mijares M. Comparison of light emitting capacitors with textured and polished silicon substrates towards the understanding of the emission mechanisms. Submitted to Journal of Luminescence. 2018 (under review)

[29] Alarcón-Salazar J. Analysis, design, fabrication and characterization of the essential devices to integrate an all-silicon photonic circuit [PhD thesis]. INAOE, Puebla, México. April 2017. DOI: http://inaoe.repositorioinstitucional.mx/jspui/handle/1009/343

[30] Spallino L, Vaccaro L, Sciortino L, Agnello S, Buscarino G, Cannas M, Mario Gelardi F. Visible-ultraviolet vibronic emission of silica nanoparticles. Physical Chemistry Chemical Physics. 2014;**16**:22028-22034. DOI: 10.1039/c4cp02995j

[31] Sopinsky M, Khomchenko V. Electroluminescence in SiO_x films and SiO_x-film-based system. Current Opinion in Solid State & Materials Science. 2003;**7**:97-109. DOI: https://doi.org/10.1016/S1359-0286(03)00048-2

[32] López-Estopier R, Aceves-Mijares M, Falcony C. Cathodo- and photo-luminescence of silicon rich oxide films obtained by LPCVD. In: Yamamoto N, editor. Cathodoluminescence. InTech; 2012. pp. 253-272. DOI: 10.5772/34888

[33] Kalnitsky A, Ellul JP, Poindexter EH, Caplan PJ, Lux RA, Boothroyd AR. Rechargeable E′ centers in silicon implanted SiO_2 films. Journal of Applied Physics. 1990;**67**(12):7359-7367. DOI: https://doi.org/10.1063/1.346059

[34] Wang M, Anopchenko A, Marconi A, Moser E, Prezioso S, Pavesi L, Pucker G, Bellutti P, Vanzetti L. Light emitting devices based on nanocrystalline-silicon multilayer structure. Physica E. 2009;**41**:912-915. DOI: https://doi.org/10.1016/j.physe.2008.08.009

[35] Quiroga-González E, Bensch W, Aceves-Mijares M, Yu Z, López-Estopier R, Monfil-Leyva K. On the photoluminescence of multilayer arrays of silicon rich oxide with high silicon content prepared by low pressure chemical vapor deposition. Thin Solid Films. 2014;**519**:8030-8036. DOI: https://doi.org/10.1016/j.tsf.2011.06.020

[36] Vinciguerra V, Franzo G, Priolo F, Iacona F, Spinella C. Quantum confinement and recombination dynamics in silicon nanocrystals embedded in Si/SiO_2 superlattices. Journal of Applied Physics. 2000;**87**:8165. DOI: https://doi.org/10.1063/1.373513

[37] Alarcón-Salazar J, Zaldívar-Huerta IE, Morales-Sánchez A, Domínguez C, Pedraza-Chávez J, Aceves-Mijares M. Enhancing emission and conduction of light emitting capacitors by multilayered structures of silicon rich oxide. Sensors and Actuators A. 2017;**265**:306-312 http://dx.doi.org/10.1016/j.sna.2017.08.047

[38] Limpens R, Lesage A, Fujii M, Gregorkiewicz T. Size confinement of Si nanocrystals in multinanolayer structures. Scientific Reports. 2015;**5**(17289). DOI: 10.1038/srep17289

[39] Alarcón-Salazar J, Zaldívar-Huerta IE, Aceves-Mijares M, Electrical and electroluminescent characterization of nanometric multilayers of SiO_X/SiO_Y obtained by LPCVD including non-normal emission. Journal of Applied Physics. 2016;**119**(21):215101. DOI: https://doi.org/10.1063/1.4952730

[40] Fu S-W, Chen H-J, Wu H-T, Shih C-F. Effect of SiO_2 layers on electroluminescence from Si nanocrystal/SiO_2 superlattices prepared using argon ion beam assisted sputtering. Vacuum. 2016;**126**:59-62. DOI: https://doi.org/10.1016/j.vacuum.2016.01.020

Chapter 3

Multifunctional Optoelectronic Device Based on Resistive Switching Effects

Hongwei Tan, Gang Liu and Run-Wei Li

Additional information is available at the end of the chapter

http://dx.doi.org/10.5772/intechopen.74826

Abstract

Optoelectronic resistive switching devices, utilizing optical and electrical hybrid methods to control the resistance states, offer several advantages of both photons and electrons for high-performance information detecting, demodulating, processing, and memorizing. In the past decades, optoelectronic resistive switching devices have been widely discussed and studied due to the potential for parallel information transmission and processing. In this chapter, recent progresses on the optoelectronic resistive switching mechanism, materials, and devices will be introduced. Then, their performance such as photoresponsivity, on/off ratio, as well as retention will be investigated. Furthermore, possible applications of the optoelectronic resistive switching considering logic, memory, neuromorphic, and image-processing devices will be summarized. In the end, the challenges and possible solutions of optoelectronic resistive switching devices for the next-generation information technology will be discussed and prospected.

Keywords: optoelectronic, resistive switching, memristor, memory, logic, neuromorphic

1. Introduction

The great success of transistor-based integrated circuits for modern computing provided exponential development of the way we live, work, and communicate. In the past decades, device scaling-down was an effective approach to maintain the continuous development of computing capabilities. However, the current semiconductor technology is facing the physical scale limitation and bandwidth bottleneck between memory and central processing unit (CPU) in modern-computing architectures, as shown in **Figure 1a**. Therefore, new devices, new architectures, and even new computing principles are eagerly desired to further enhance computing efficiency and capability in the post-Moore era.

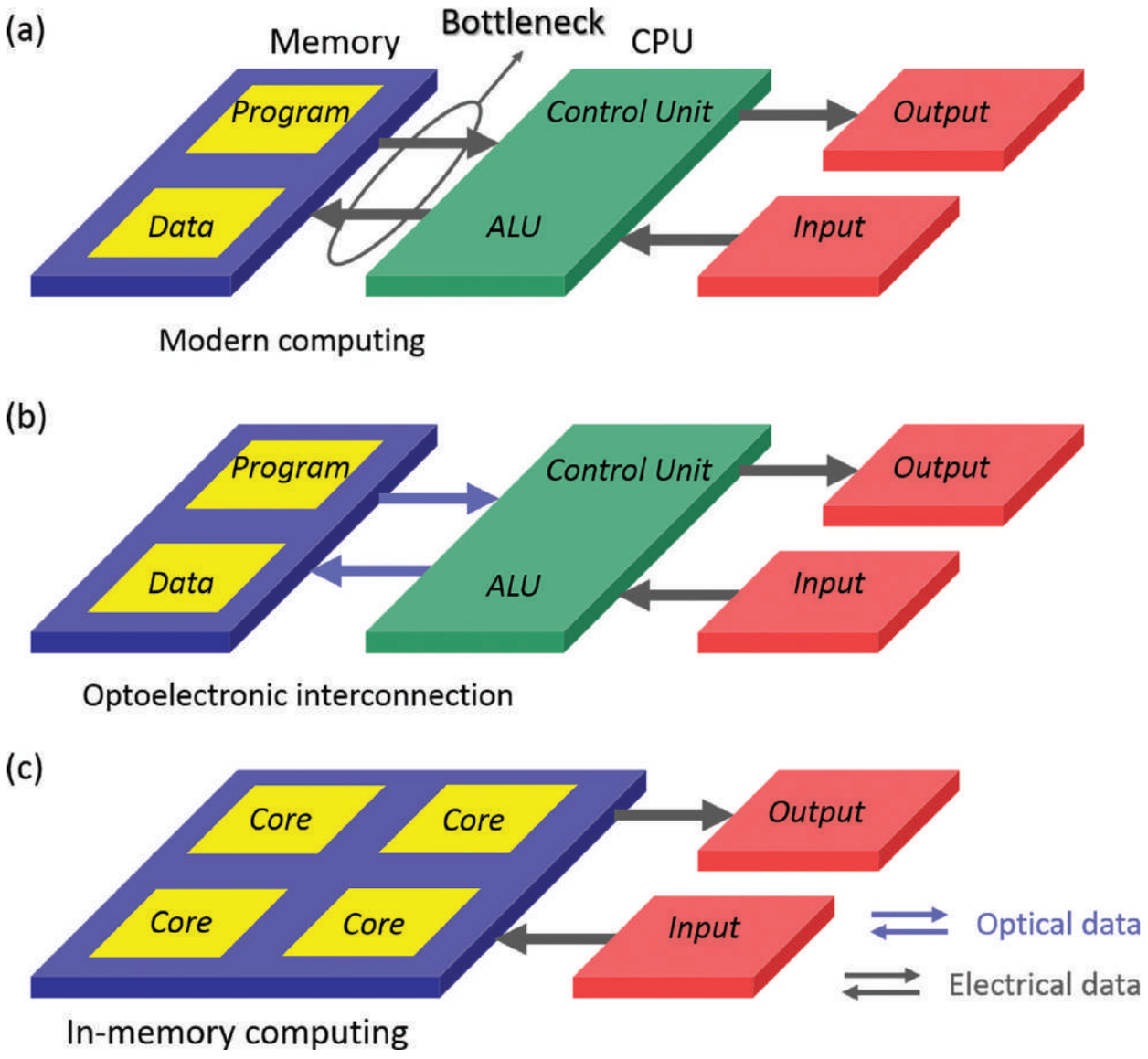

Figure 1. Possible approaches to optimize computing architectures. (a) Modern von Neumann-computing architecture. The separated memory and CPU are connected by data bus, which has frequency limitation. This architecture has low efficiency in data processing between memory and CPU. (b) Optical communication between memory and CPU will overcome the frequency limitation and increase its efficiency. (c) Parallel data processing and memory using memristor-based architecture.

Optoelectronic interconnection is a feasible method to overcome the bottleneck by transmitting data between memory and CPU *via* photons, which have a much faster transporting speed, a higher bandwidth, no Joule heat, and no interference over electrons [1–10]. As shown in **Figure 1b**, optical communication between CPU and memory will fully meet the demands of modern-computing architecture in high-frequency data communicating and processing [1–10]. On the other hand, memristor (memory + resistor), a simple two-terminal electrical switch with nonvolatile reconfigurable resistance states, has been considered as one of the promising approaches to construct new architecture with the novel in-memory computing (**Figure 1c**) [11–20]. Due to the arbitrary nonvolatile resistance states, memristor-based architectures provide the

high potential for integrating processor and memory together, which eliminates the bottleneck between memory and processor in the modern von Neumann-computing architecture, thus allowing high parallel data processing [21–26]. However, the electronic memristor-based architecture still has bandwidth limitation in high-frequency data communicating between different modulators.

The combination of photons and memristor-based circuits will integrate the advantages of photons in a high-speed data transmission and memristors in parallel in-memory computing and may open up a new era for future computing owing to the high bandwidth and low-power consumption. Moreover, the optoelectronic-based memristive system will extend the application of memristor-based architecture to image or visual information processing. As shown in **Figure 2**, with the increasing demands of mobile computing in human daily life, wearable devices, health-care devices, and human-machine interacting devices including intelligent image sensor, video monitor, invisible touch screen, electronic eyes, wearable heart or blood monitoring and display devices, smart processor, and even brain-implantable devices will be more and more important for an efficient and comfortable way for our better life, body health, daily work, and communication [27–32]. The optoelectronic memristor-based architecture, wherein both photons and electrons are used for parallel data processing and communicating between input-output (I/O) devices and the in-memory processor, may provide such a platform for the mobile computing.

In this chapter, recent developments on optoelectronic memristor materials and devices, and applications including logic, memory, memristor, and neuromorphic devices will be summarized, then their capability in future optoelectronic on-chip interconnection, in-memory computing, brain-inspired computing, and visual information processing will be evaluated.

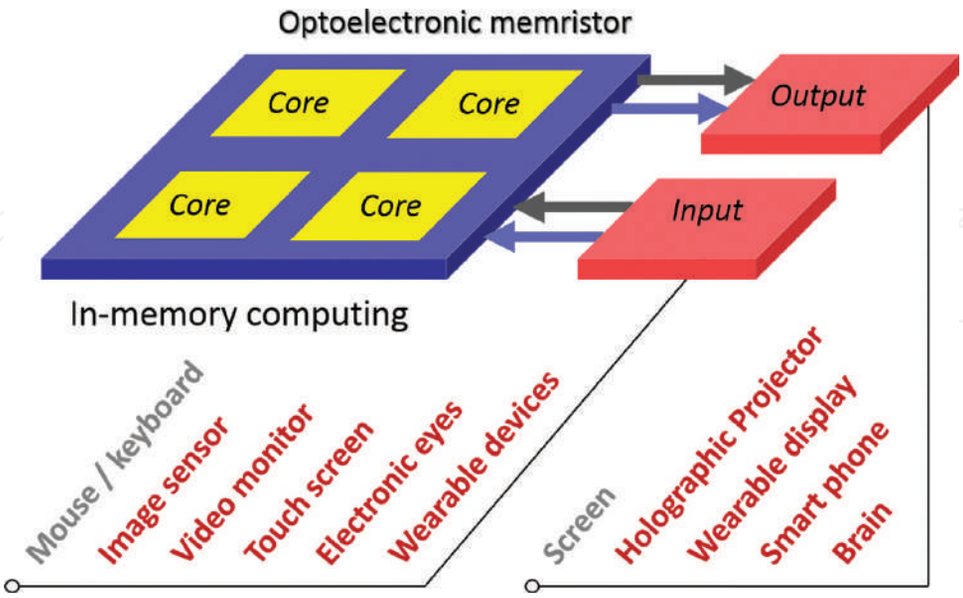

Figure 2. Possible optoelectronic memristor-based-computing architecture. In the in-memory processing unit, a core has the ability to process and store data *in situ*. Both photons and electrons can achieve the communication between the cores and I/O devices.

These optoelectronic approaches may help to overcome the limitations and bottleneck in the current computing devices and architectures, as well as contribute to efficient data analysis, cognitive computation, and artificial intelligence.

2. Optoelectronic resistive switching materials and devices

Resistive switching memory (memristor) is a simple two-terminal device with three-layered structure—two electrode layers for electrical signals input and output, and a "memory" layer in between. The resistance of the "memory" layer can be dynamically reconfigured by voltage- or current-induced ion implantation, interfacial charge accumulation, and so on. Usually, the electrodes are metal or oxide, such as Ag, Au, Pt, Ta, Ir, Cu, ITO, and so on, which will affect the resistive switching behavior by their different work function, electron affinity, electrochemical energy, and so on [33, 34]. For the "memory" layer, various kinds of materials have been used, including binary oxide, nitride, perovskite, low-dimensional materials, and organic materials [35–45]. Due to the simple structure and excellent performance including high-density integration, high-speed, and low-cost fabrication for logic, memory, and neuromorphic applications, memristor has been considered as one of the most promising next-generation information technologies [19, 20, 46].

Meanwhile, optical interconnection with high data transmission speed and no Joule heat or interference has proved to be another effective approach to overcome the data transmission bottleneck between memory and processor. Moreover, combining the advantages of photons and electrons in an optoelectronic memristor will allow highly parallel data transmission and processing, as well as extending the application for image recognition and visual information processing. In the optoelectronic memristor (**Figure 3**), both optical and electrical signals are able to modulate the resistance states of a "memory" layer, which is sensitive to both electrical

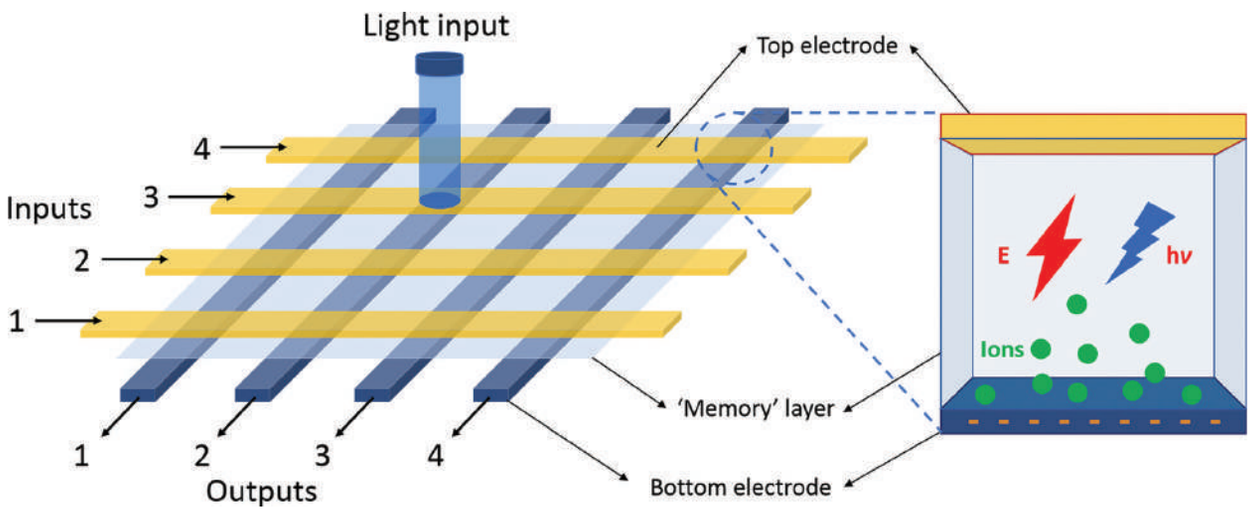

Figure 3. Optoelectronic memristor structure and mechanism.

and optical signals. Therefore, photosensitive semiconductor materials will meet the demands of the "memory" layer, such as silicon, cerium oxide, zinc oxide, perovskite, low-dimensional materials and organic materials, and so on [47–52].

In 2012, Ungureanu et al. reported a reversible light-controlled resistive switching memory in metal/Al_2O_3/SiO_2/Si structure, with the photogenerated electrons injection from Si to Al_2O_3 at sufficient positive bias and charge removal at negative bias [53]. In this work, the light pulses with different wavelength and intensity were utilized to study the photoresponsive behavior of the memory, as well as to achieve multilevel and multifunctional optoelectronic resistive switching memory. This work proved that the metal/Al_2O_3/SiO_2/Si-structured device can work as a multifunctional optoelectronic device including information storage and light sensing, meanwhile, offering the possibility for extra optical degree to be exploited in resistive switching memory devices.

Besides Si, ZnO is another kind of typical photosensitive semiconductor and has been widely studied for UV detectors, as well as resistive switching memories [35, 49]. Based on the semiconducting and photosensing properties of ZnO, Bera et al. combined the resistive switching and persistent photoconductivity (PPC) together in ZnO/NSTO Schottky junction in 2013 [54]. The photo-induced interfacial positive oxygen vacancies movement under electric field can lower the interfacial barrier and modulate the nonvolatile multilevel resistance states, thus realizing persistent photoconductivity and resistive switching. Annealing process was able to erase the PPC to its initial state. The results in this work provided a general route to achieve multifunctional devices by integrating functional materials.

Most recently, two-dimensional materials, such as graphene and MoS_2, have drawn much more attention due to their promising properties for the next-generation information technology. In 2014, Roy et al. reported a multifunctional photoresponsive memory based on graphene-MoS_2 hybrid three-terminal structure, wherein a gate was used to maintain and erase the trapped charges, thus achieving erasable persistent photoconductivity for optoelectronic memory devices (**Figure 4**) [55]. In addition, different gate amplitudes and light intensities were used to achieve multilevel memory. This work showed that the novel two-dimensional materials are promising for multifunctional optoelectronic memory.

Besides, organic materials have many advantages including low-cost fabrication, flexibility, and bandgap tunability, which are promising for optoelectronic memory devices. In 2012, Ye reported an optoelectronic multilevel resistive switching memory shown in **Figure 5** using a metal-conjugated donor-bridge-acceptor (DBA) molecule, which is responsive to both optical and electrical stimuli [56]. Under dark condition, the Al/metal-conjugated DBA/ITO-structured devices showed a bi-stable resistive switching behavior. When illuminated by UV light, a middle state was induced by the sub-step charge transfer process through the cooperation of UV light and electric field. This work may open up new opportunities of organic materials for designing multifunctional optoelectronic memory.

In a short summary, photo-induced charge trapping and detrapping play the key role in optoelectronic resistive switching effect. Other than the materials stated earlier, carbon nanotube, complex oxide, perovskite, quantum dots, and so on, also show optoelectronic resistive

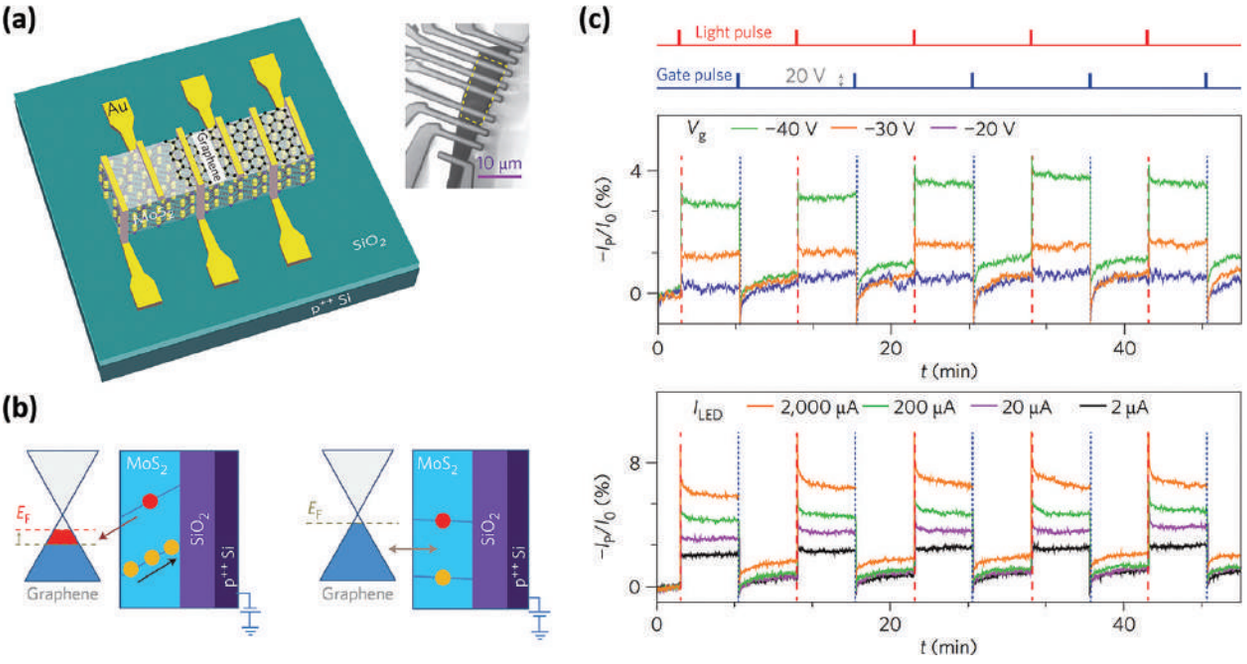

Figure 4. Photosensitive memory based on MoS_2/graphene hybrid structure. (a) Materials and devices structure. (b) Photoresponse mechanism. (c) Multilevel optoelectronic memory via modulating gate bias and light intensity. Reproduced with permission from Ref. [55]. Copyright 2014 Nature Publishing Group.

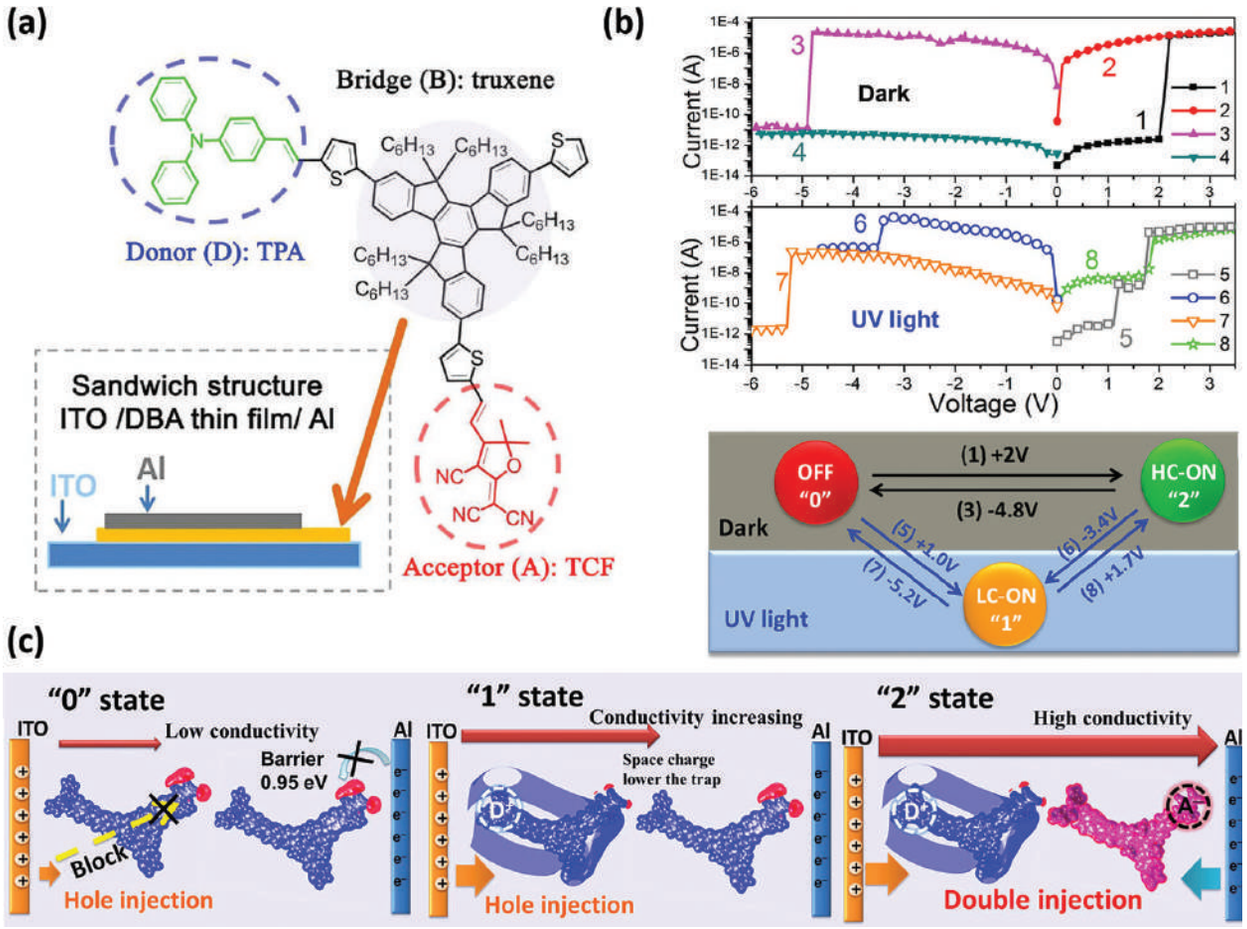

Figure 5. Organic optoelectronic resistive switching memory. (a) Materials and devices structure. (b) Resistive switching behaviors under dark and UV light illuminations. (c) Optoelectronic switching mechanism. Reproduced with permission from Ref. [56]. Copyright 2012 American Chemical Society.

switching effects [57–60]. The applications of optoelectronic memristor including logic, memory, neuromorphic devices, and their performance will be discussed in the following sections.

3. Multifunctional optoelectronic logic and memory

Optoelectronic memristors, allowing electrical and optical signals to modulate the states, are capable of functioning as sensor, decoder, arithmetic unite, logic, and memory devices for data communication, integrated photonics, in-memory computing, and brain-like computing. In this section, optoelectronic logic and memory devices will be discussed and their performance will be evaluated.

Logic is one of basic and most important functions in the integrated circuits [61–65]. Therefore, the realization of optical and electrical-mixed logic is the first step for optoelectronic circuits. For example, Kim et al. reported a series of optoelectronic logic devices based on single-walled carbon nanotube (SWNTs)/silicon junctions [57]. As shown in **Figure 6a**, in the SWNTs/Si junction, voltage and light pulse are inputs and currents are outputs. Due to the photoresponse under voltage bias, the output current is much higher (logical "1") when both voltage and light are applied to the junction than the current when only one or neither is applied (logical "0"), thus functioning as an "AND" gate (**Figure 6b**). Similarly, "OR" gate and 2-bit adder functions were also achieved using two junctions. Furthermore, utilizing four junctions with specialized

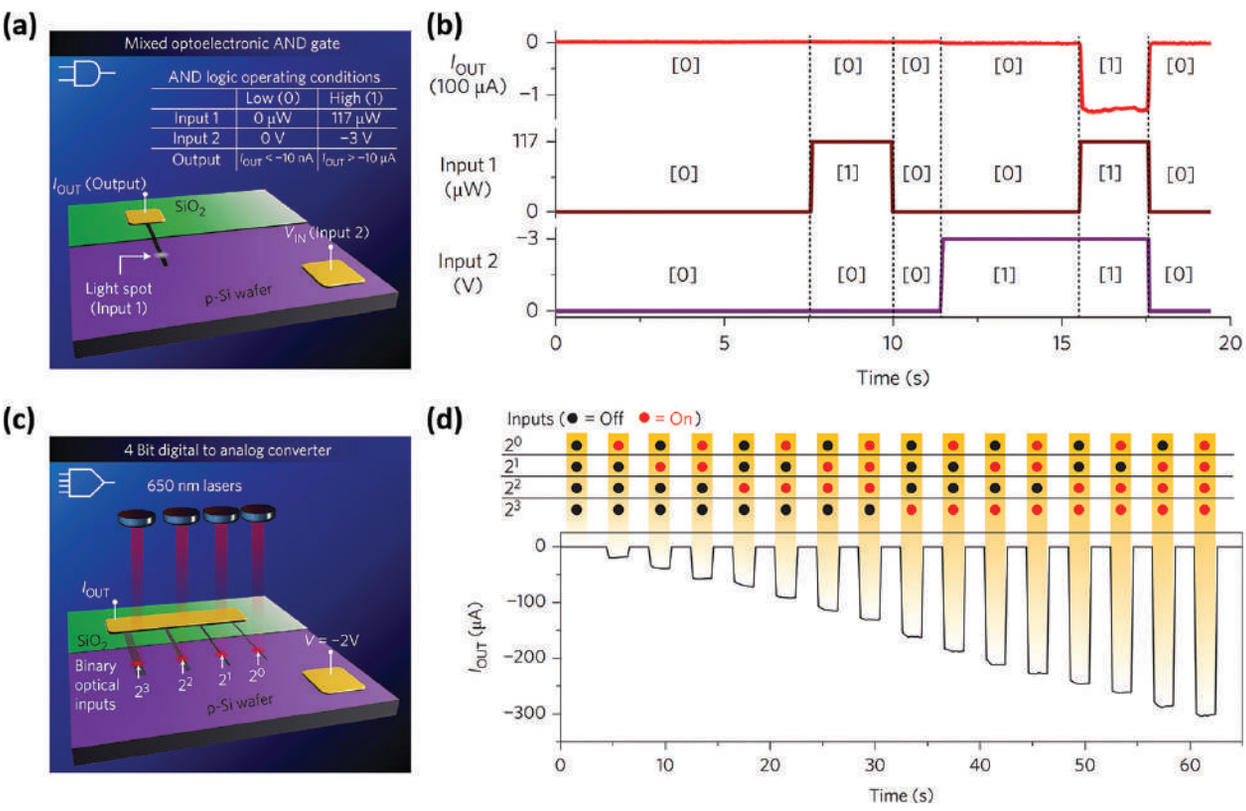

Figure 6. Optoelectronic logic gates. (a) "AND" logic with one light input, one voltage input, and a current output. (b) Output current value of the "AND" gate. (c) 4-bit digital-to-analog converter with light illuminating on four junctions with different areas. (d) Output current value of the 4-bit digital-to-analog converter. Reproduced with permission from Ref. [57]. Copyright 2014 Nature Publishing Group.

active areas, a 4-bit digital-to-analog converter (DAC) was demonstrated, as shown in **Figure 6c** and **d**.

Memory is another basic and important function in integrated circuits. If an optoelectronic memory device can integrate other specific functions such as photo signal detection, demodulation, arithmetic, and even logic in a single device, where the processed data can be stored *in situ*, then it will lower the complexity of integrated circuits and allow highly parallel computation. To achieve this goal, in 2015, we studied the ITO/CeO_{2-x}/AlO_y/Al-structured photoresponsible junction and designed a multifunctional optoelectronic resistive switching memory (OE-memory) with integrated photodetection, demodulation, and arithmetic [66]. As shown in **Figure 7**, CeO_{2-x} works as a photon-absorbing layer, and the electrons trapped in the defects in the CeO_{2-x} layer near the interface can be excited by photons and leaving positively charged oxygen vacancies, which will lower the effective barrier and decrease the resistance of the junction persistently with a thinner barrier. At the CeO_{2-x} and Al interfaces, a 5-nm native oxide layer formed and acted as an insulating layer to decrease the dark current. ITO works as a transparent and conductive top electrode and Al is the bottom electrode. In this simple two-terminal structure, persistent photoconductivity was observed as shown in **Figure 8**. The nonvolatile resistance states can be reversibly switched between high resistance state (HRS) and low resistance state (LRS) by visible light pulse and voltage, thus acting as an optical-write and electrical-erase memory.

Further study of this optoelectronic memory showed the wavelength and intensity-dependent photoresponse, which was utilized to design an optical signal detector and demodulator. As shown in **Figure 9**, with two-digit information (wavelength and intensity) per light pulse, four pulses with blue or green and 4 or 6 pW/μm^2 are capable of carrying

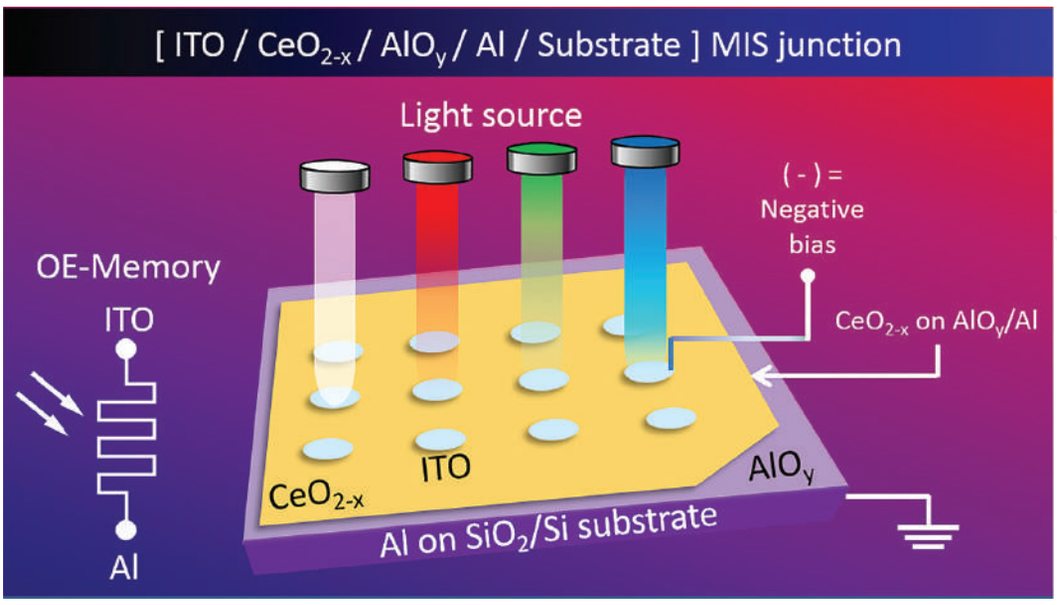

Figure 7. Schematic illustration of the optoelectronic memory (OE-memory) based on the ITO/CeO_{2-x}/AlO_y/Al junction and its operation principle. Reproduced with permission from Ref. [66]. Copyright 2015 WILEY-VCH Verlag GmbH & Co. KGaA, Weinheim.

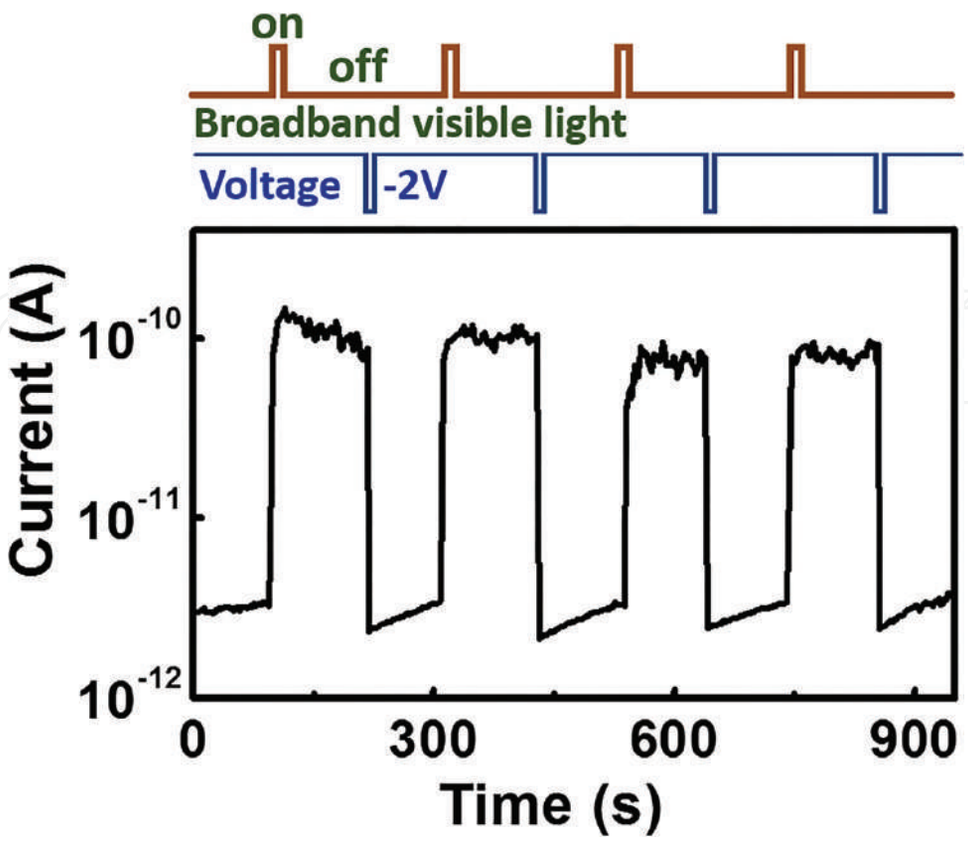

Figure 8. Reversible nonvolatile optoelectronic resistive switching behavior. A visible light pulse switches the structure from HRS to LRS and a voltage pulse switches the structure from LRS to HRS. Reproduced with permission from Ref. [66]. Copyright 2015 WILEY-VCH Verlag GmbH & Co. KGaA, Weinheim.

8-digit information, which is one letter according to the ASCII code, and can be demodulated and stored into four resistance states. Therefore, optical signal detecting and demodulating functions have been achieved in this simple optoelectronic memory. Furthermore, the photoconductance is increasing linearly with light pulse number (**Figure 10a**). Based on this linear relationship between photocurrent and the number of light pulses, counter and adder of the number of light pulses can be realized and the details are shown in **Figure 10b**. Meanwhile, the output results after counting or adding the pulse number can be stored as resistance states, thus allowing the integration of simple arithmetic and memory functions in a single cell. To evaluate the memory retention performance, multilevel resistance states were measured continuously, and after 10^4 s, the resistance states remain distinguishable (**Figure 11**). Above all, the simple optoelectronic structure is capable of functioning as optical signal detection, demodulation, arithmetic, and storage. These results demonstrate the possibility of using multifunctional optoelectronic devices for future integrated photonics, parallel processing, and in-memory computing [66].

In our recent work, to further exploit the integration of logic functions into the memory [67], electrically resistive switching and the persistent photoconductivity are combined to modulate the resistance states (**Figure 12**) [68].

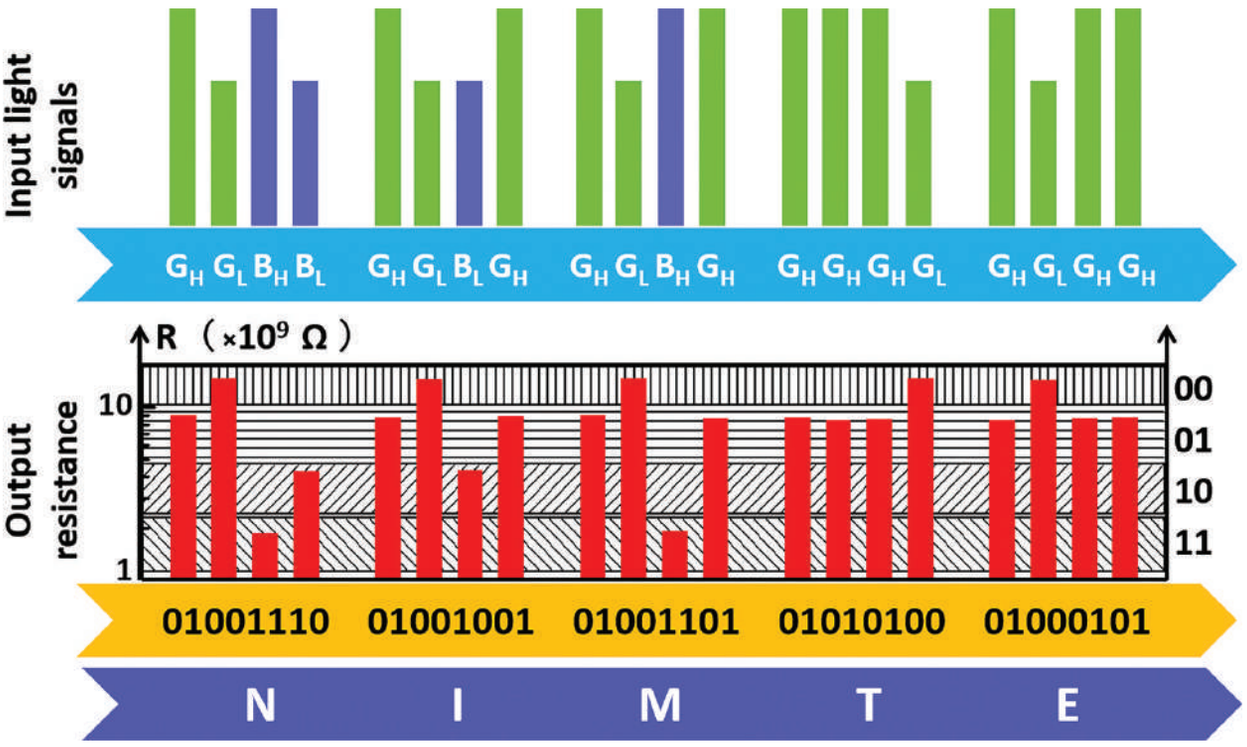

Figure 9. Proof-of-concept demonstration of demodulating function. The work "NIMTE" encoded in light pulses according to ASCII code can be demodulated and stored into nonvolatile resistance states.

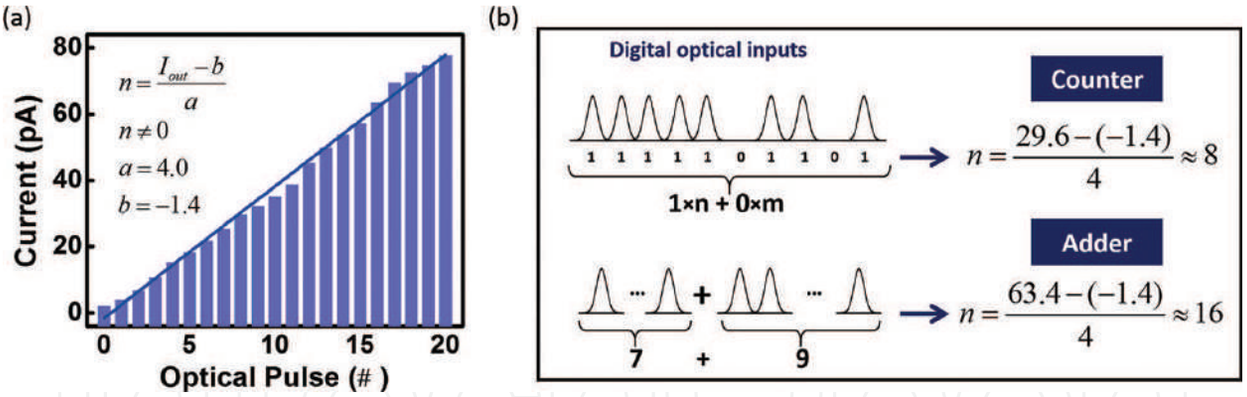

Figure 10. Optoelectronic arithmetic function in the OE-memory. (a) Photocurrent after a series of identical light pulses. (b) Simple counter and adder functions demonstration based on the linear relationship between photocurrent and light pulse number shown in (a). Reproduced with permission from Ref. [66]. Copyright 2015 WILEY-VCH Verlag GmbH & Co. KGaA, Weinheim.

Using one light pulse and one voltage pulse as logical inputs and current as logical output, an "AND" gate was achieved. Only when both a light pulse and a voltage pulse are present, the output value is larger than 150 nA, which is logical "1," otherwise, the output current is lower than 150 nA, which is logical "0." Furthermore, the "AND" gate can be reconfigured to "OR" gate when a light-write pulse applied before logic operations, thus allowing the OE-memory functioning as an optoelectronic nonvolatile reconfigurable logic gate (**Figure 13**). Besides the reconfigurable "AND" and "OR" logic functions, "NOT" operation and a complicated logic operation were achieved by introducing another electrical-erase pulse, as well as optical adder

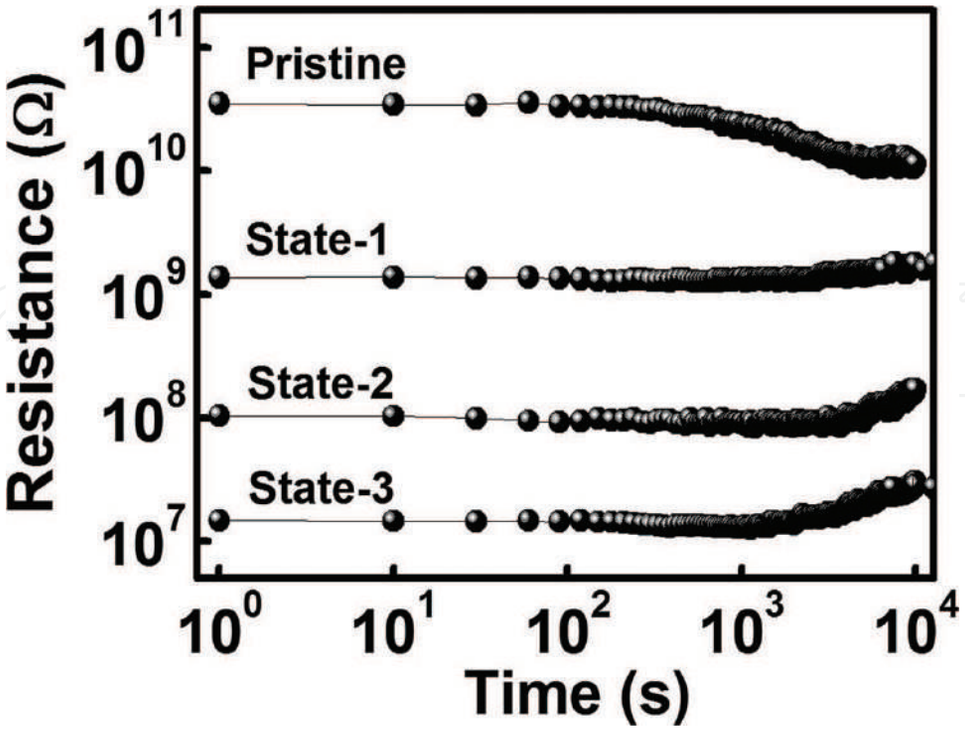

Figure 11. Retention characteristic of four states programmed by light pulses with different intensities. Reproduced with permission from Ref. [66]. Copyright 2015 WILEY-VCH Verlag GmbH & Co. KGaA, Weinheim.

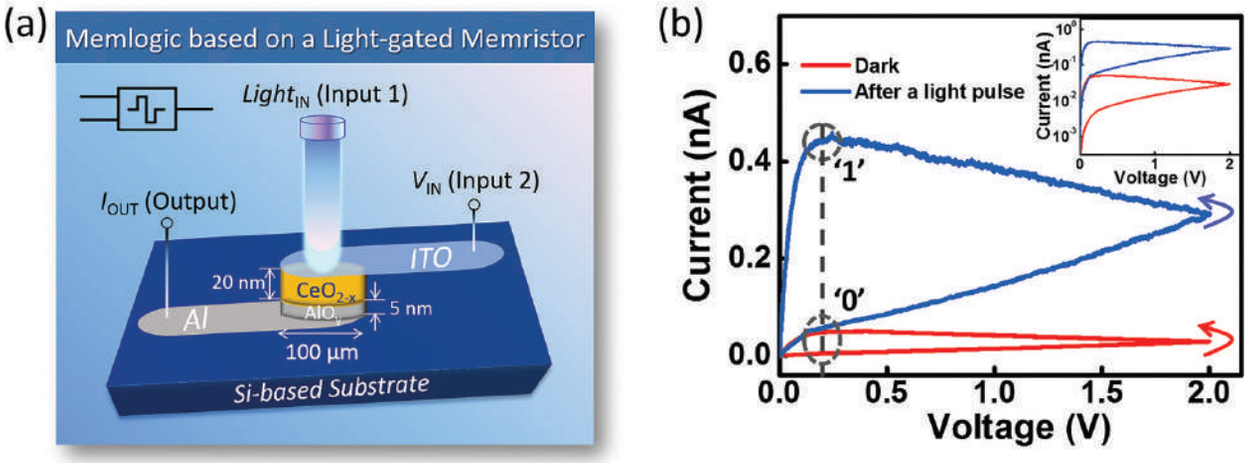

Figure 12. Schematic illustration of the structure (a) and optoelectronic resistive switching behaviors (b) of the memlogic. Reproduced with permission from Ref. [68]. Copyright 2017 American Chemical Society.

and digital-to-analog converter (DAC) functions were achieved by using two light pulses as inputs. We name this nonvolatile reconfigurable logic gate as "memlogic," memory of logic operations and outputs.

Based on the optoelectronic reconfigurable logic functions, a proof-of-concept reconfigurable image-processing and memorizing functions were demonstrated, as shown in **Figure 14**. Two images with "X" and "Y" shapes of visible light pulses are used as inputs into a 5 by 5 memlogic array and current map as output (**Figure 14a**). When all the cells were reset to "AND" logic state,

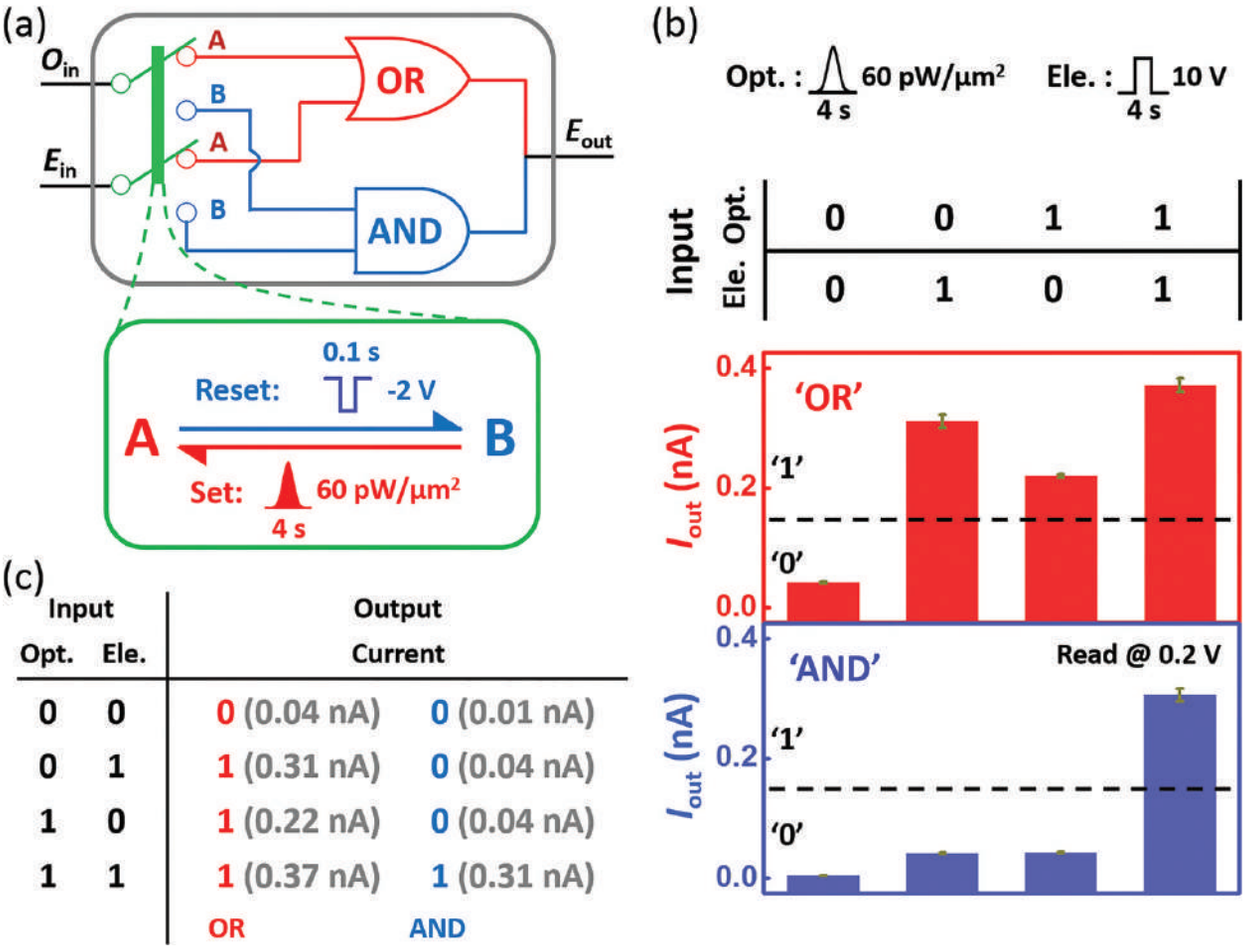

(c)

Input		Output	
Opt.	Ele.	Current	
0	0	0 (0.04 nA)	0 (0.01 nA)
0	1	1 (0.31 nA)	0 (0.04 nA)
1	0	1 (0.22 nA)	0 (0.04 nA)
1	1	1 (0.37 nA)	1 (0.31 nA)
		OR	AND

Figure 13. Memlogic operation of reconfigurable "AND" and "OR" gates. (a) Reconfiguration operation of "AND" and "OR" gates. (b) Output current value of the memlogic. (c) Truth table of the memlogic. Reproduced with permission from Ref. [68]. Copyright 2017 American Chemical Society.

the processor can find the same part in different images and we named it SAME FINDER (**Figure 14b**). When all the cells were set to "OR" states, the processor can find the parts either in 'X" or "Y" images and we named it as ALL FINDER (**Figure 14c**). Therefore, the single memlogic array can realize two different image processing, as well as image storage functions.

Above all, the memlogic is capable of performing different reconfigurable logic functions and nonvolatile memory and may provide a new method for reconfigurable in-memory computing, integrated photonics, and artificial intelligence [68].

In summary, for information technology application, these optoelectronic resistive switching devices need to be optimized to improve their performance including the photoresponsivity, speed, memory window, retention time, endurance, fabrication cost, reliability, yield, and so on. Here, the summary of some basic parameters is shown in **Table 1**. The photoresponsivity measures the input–output gain in a photoresponsive system and means the electrical output per optical input. On/off means the memory window. Speed represents how fast the device can work. For memory or logic applications, the speed needs to be at ns level. Here, the speed of these optoelectronic resistive switching devices is not enough and needs to be improved exponentially. Possible methods will be increasing the build-in electric field to accelerate the

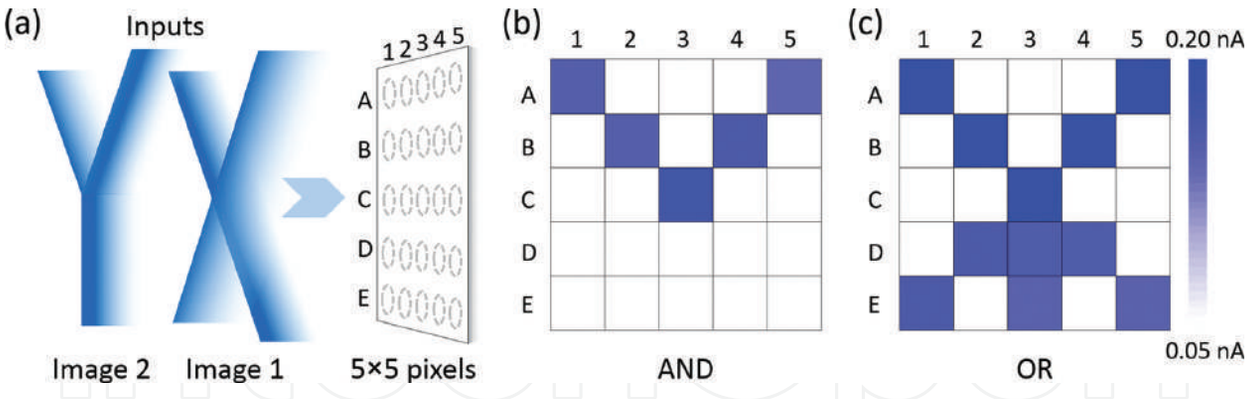

Figure 14. Proof-of-concept demonstration of reconfigurable image processing. (a) 'X' and 'Y" shape of light image were inputs and current map was the output. (b) Image same finding function when all the memlogic cells are at HRS and (c) image all finding functions when all the memlogic cells are at LRS. Reproduced with permission from Ref. [68]. Copyright 2017 American Chemical Society.

Structure	PPC/PC/PR	Responsivity	On/off	Speed	Retention	References
$Pd/Al_2O_3/SiO_2/Si$	PC	_	10^3	_	_	[53]
Ti/ZnO/NSTO	PPC	_	$>10^3$	~100 s	$>10^4$ s	[54]
Al/Organic/ITO	PR	_	10^6	_	5×10^4 s	[56]
$ITO/CeO_{2-x}/AlO_y/Al$	PPC	1 A/W	10^3	~10 s	$\sim 10^4$	[66, 68]

Notes: PPC, persistent photoconductivity; PC, photoconductivity; PR, photoresponse.

Table 1. Characteristics of the typical photoresponsive memristors.

photo-induced charge separation by using electrodes with a higher work function or increasing the defects concentration. Retention means how long the state can maintain. From this table, we can see that the performance especially the speed should be improved immediately.

4. Optoelectronic neuromorphic devices

Artificial neural network is one of the most promising ways to achieve brain-like computing and has been an attractive area especially for memristors as the similar ionics-based mechanisms and stochastic dynamics with neurons [69–87]. Optoelectronic memristors provide another degree of freedom by light to control their states, which means light pulse can be utilized as stimuli to control artificial synapse weight and proceed with synaptic behaviors simulation. Moreover, optoelectronic memristor-based networks allow optical communications among nodes and will reduce power consumption, increase communicating speed, and efficiency. Recently, several research groups have proposed optoelectronic artificial synaptic devices based on persistent photoconductivity for neuromorphic computing. In 2010, Agnus et al. reported an adaptive architecture based on optically gated carbon nanotube transistors, which allow optical write and electrical program processes to control the resistance states [88]. The programmed states are nonvolatile and can be used to store synapse weight in adaptive architectures. More specific synaptic behaviors simulation such as short-term memory (STM), long-term memory (LTM),

facilitation, and spike-timing-dependent plasticity (STDP) have been achieved in IGZO-based persistent photoconductive devices by Lee in 2017. They also showed the photoenergy and frequency-dependent plasticity. These basic synaptic behaviors simulation will promote the development of optoelectronic artificial neuro-network [88].

As we all know, human eyes are the most important media to receive visual information from surroundings and provide humans with the ability to recognize objects. In human visual system, the eyes receive light signal and convert it to electrical pulses signal, which can be detected by visual neuron and analyzed or memorized by visual cortex in the brain. In general, two parts for sensing and processing of visual information form the visual system. In recent years, inspired by human visual system, several kinds of artificial visual systems have been proposed to simulate eyes for visual information processing, retinopathy therapy, and reproduction of visual system [27, 89–91]. Usually, photodetector array acts as the retina to sense the light that converts it to electrical signal for image processor, visual neuron, and cortex. For example, as shown in **Figure 15**, Mathieson et al. reported a photovoltaic retinal prosthesis, which is capable of detecting light signal, imaging on silicon photodiode array, and processing the detected image. The demonstration of fully integrated wireless implant may reproduce the vision to the patients with retina diseases [27]. However, this photodiode-based system lacks the function of memorizing of image information. Therefore, memristor may be applicable for image memory. In 2017, Chen et al. reported an artificial visual memory system consisting of an imager and a memory. The UV image can be detected by In_2O_3-based imaging system and stored by Al_2O_3-based

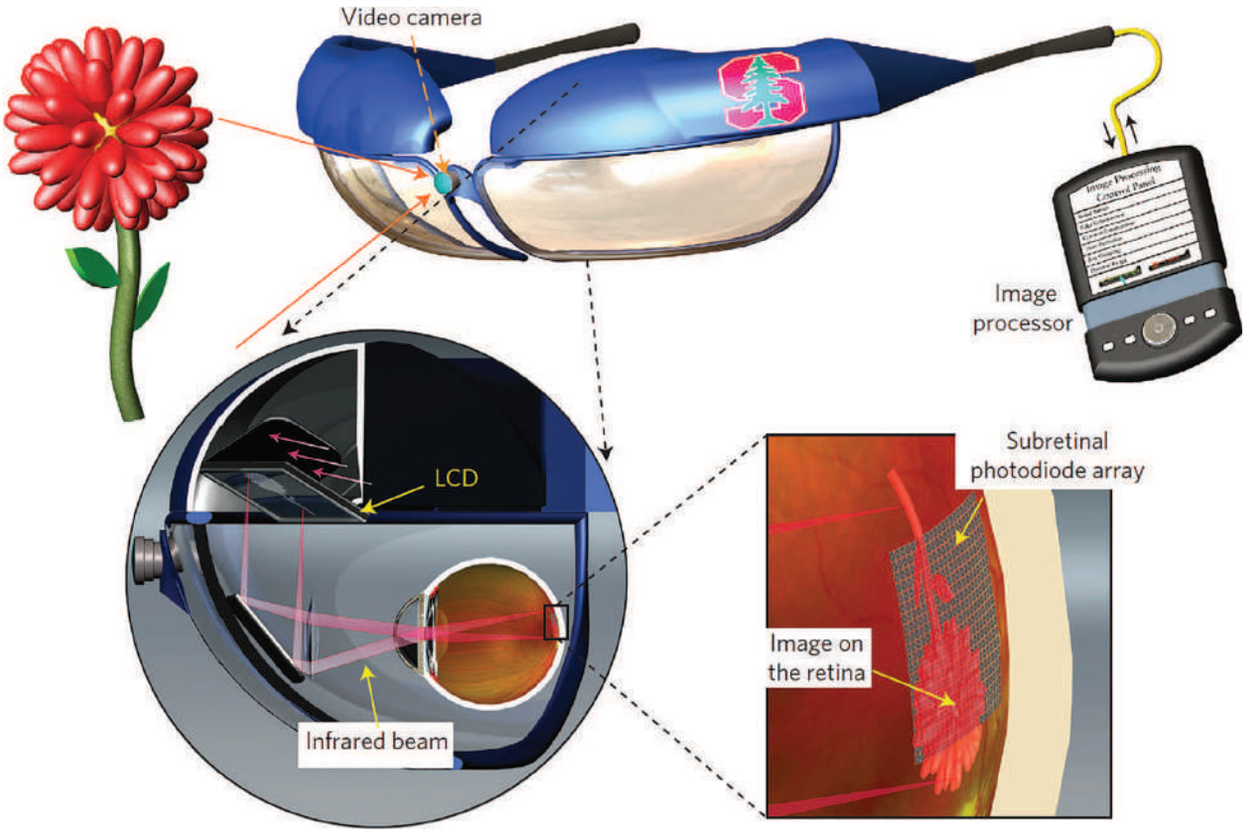

Figure 15. An artificial visual system based on silicon photodiode. Reproduced with permission from Ref. [27]. Copyright 2012 Nature Publishing Group.

processing and memory system [92]. The design of this artificial visual system provides a novel approach to integrate different devices to achieve more multifunctional bioinspired systems.

Thanks to the reported works, these novel promising optoelectronic synaptic devices have been proposed and achieved and will be the first step for optoelectronic neural networks. Optoelectronic artificial neural networks provide the additional advantage of optical communication into memristor-based neuromorphic architectures. Based on the previous research, the next plan should focus on improving their performance, exploiting optoelectronic artificial neural networks, and optogenetic neural networks.

5. Other approaches for multifunctional resistive switching

Besides the optical-based resistive switching memories, electrical- and magnetic-based resistive switching devices are also interesting and attractive due to their important and promising physical properties and applications [93].

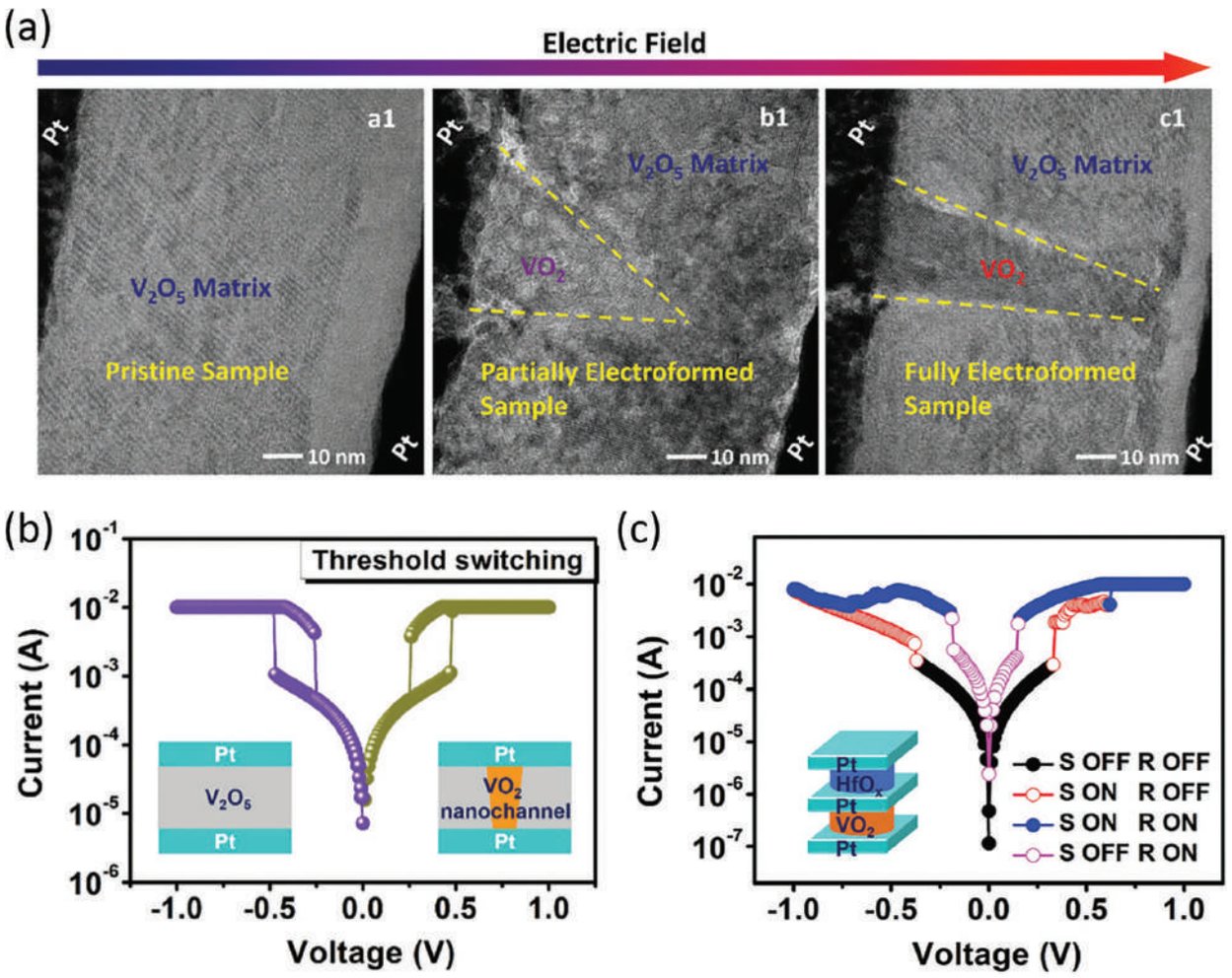

Figure 16. Nanochannel-based selector mechanism and its performance. (a) Transmission electron microscopic (TEM) image proved the electric field-induced VO_2 nanochannel formation in V_2O_5 matrix. (b) Threshold switching behavior. (c) Resistive switching behavior of the 1S1R structure. Reproduced with permission from Ref. [94]. Copyright 2017 WILEY-VCH Verlag GmbH & Co. KGaA, Weinheim.

Recently in our group, a nanochannel device was designed in V_2O_5-based selector via electric field-induced ion migration [94]. As shown in **Figure 16**, this electric field-induced nanochannel demonstrates a sharp and reliable metal–insulator transition (MIT) with a 17 ns switching speed, an 8 pJ energy consumption, and less than 4.3% variability. By combining with one HfO_x-based memristor, the 1S1R structure device can ensure the correct reading of the memory states continuously for 10^7 cycles, therefore demonstrating its great possibility to overcome the crosstalk problem in high-density crossbar memory. This work proved that electric-field-induced ion migration at the nanoscale is an effective approach to optimize device performance or design novel conceptual devices.

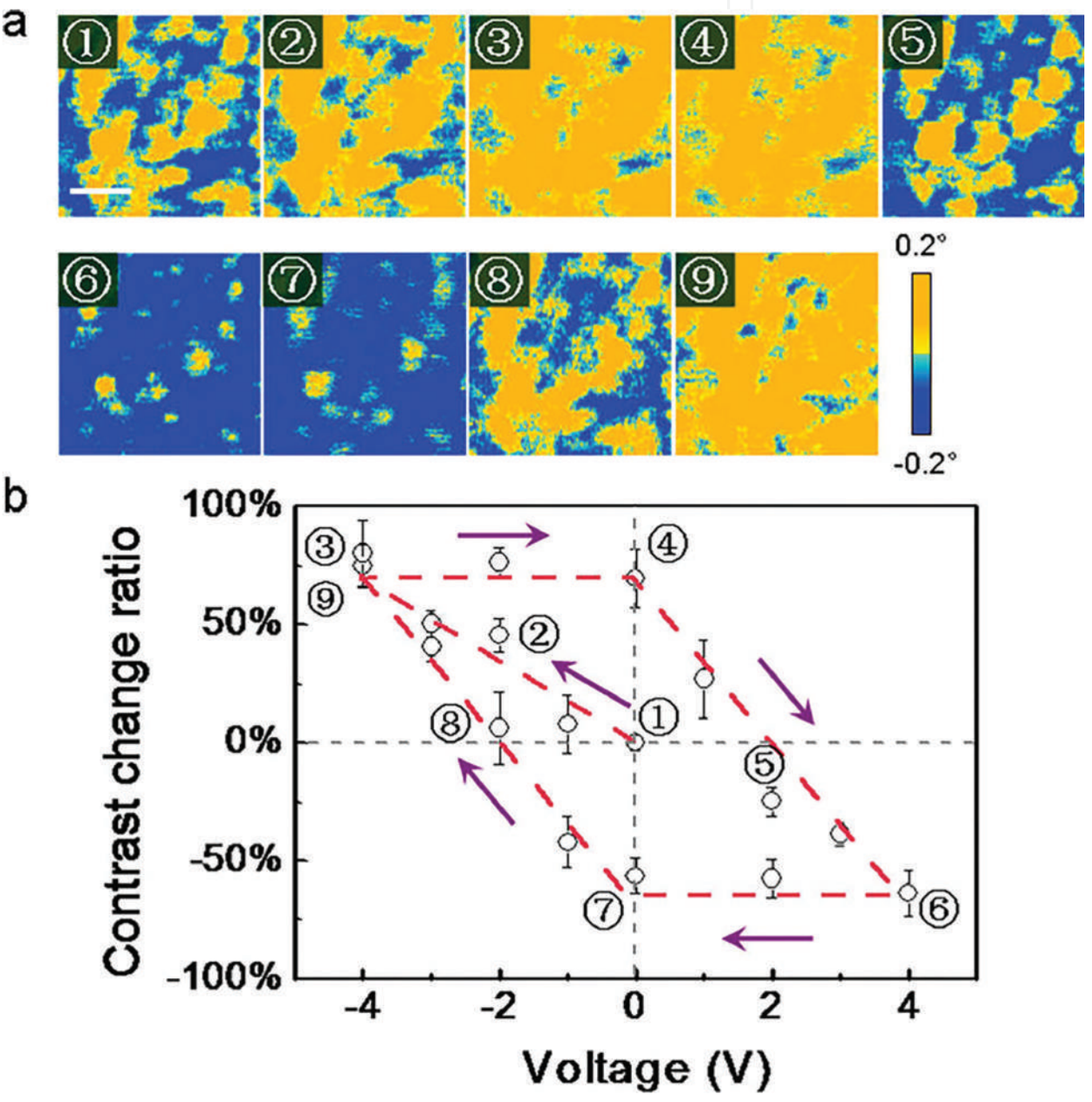

Figure 17. Electric field-controlled magnetization reversal. (a) Magnetic force microscope (MFM) images of the CFO at initial states and after voltage bias. (b) Evolution of the contrast change ratio after being subjected to various biased voltages. Reproduced with permission from Ref. [95]. Copyright 2015 American Chemical Society.

With the electric field-induced ion migration method, our group also achieved nanoscale magnetization reversal in cobalt ferrite (CFO) thin film (**Figure 17**) [95, 96]. The electric field-induced migration and redistribution of Co^{2+} between Fe vacancies induced the unidirectional magnetic anisotropy of the sample along the <110> directions. The reported magnetization reversal is nonvolatile and reversible, which can be controlled by tuning the electric field polarity and amplitude. Such a nanoscale magnetization modulation by nanoionics may provide a novel approach to manipulate the magnetization of magnetic materials for low-power magnetic memory and spintronics.

6. Challenges and possible approaches

Thanks to the efforts of scientific researchers and engineers from all over the world, the optoelectronic resistive switching has achieved great progress. However, there are still some challenges in the way of further development of optoelectronic memristors currently as follows:

1. Mechanism: the widely accepted mechanism of PPC is the photo-induced charge trapping and detrapping in defects. However, due to the technique limitation of directly mapping photo-generated carriers' distribution under light illumination, it is hard to clarify the PPC at electron scale.
2. Materials and performances: many materials are photoresponsive and resistance switchable. Therefore, finding a durable, reliable, and CMOS-compatible material with excellent optoelectronic resistive switching performances is still a challenge, and the performance especially the speed is more challenge due to defects-related process.
3. Spatial design of the optoelectronic neural networks: optoelectronic platform will need to integrate light source to the integrated circuits. Therefore, the devices' surface and physical position should be accessible for light source. Then the best way to route the light source to devices' surface is a critical issue.

Possible approaches include the following:

1. Mechanism: light-integrated TEM is a possible method to observe the light-controlled physical properties. In my current group in Finland, an *in situ* TEM under external electric field and light sources is ready, and there may be some promising results about optoelectronics in the following years [97].
2. Materials and performance: the direct and effective way to find a suitable material is trying and trying. One promising material has to be tested, optimized, and improved repeatedly before the product, and what we can do is to just be patient. The performance requirement depends on the application, so performance is negotiable [17].
3. Spatial design of the optoelectronic neural networks: with the development of nanophotonics and nanolasers, in the near future, integrated photonics will provide efficient and feasible approach to address the spatial design of optoelectronic artificial neural networks [6].

7. Conclusions and prospects

In this chapter, recent progress on optoelectronic resistive switching are introduced and summarized. Due to the photosensitive media in memristor, light can be used as another degree of freedom to control the resistive switching behavior for multifunctional optoelectronic devices. Here, the main mechanism is the photo-induced carriers trapping and de-trapping in defects in the semiconductor "memory" layer. To further promote the development of the multifunctional optoelectronic devices, their performance should be improved to meet different applications considering image sensor, memory, logic, and neuromorphic devices.

Optoelectronic memristor-based neuromorphic devices, integrating the functions of information storage, processing, image detection, and memory together, may provide high potential for intelligent image sensor and optoelectronic in-memory computation. Based on the integrated photonics [1–10], optoelectronics [47–60], and optogenetics [98–100], an optoelectronic artificial neural network may play a key role in future human-machine interactive devices.

Acknowledgements

This work was supported by the National Key R&D Program of China (2017YFB0405604), the National Natural Science Foundation of China (61722407, 61674152, 51525103, 11474295), the Natural Science Foundation of Zhejiang Province (LR17E020001), and the Youth Innovation Promotion Association of the Chinese Academy of Sciences (2014261).

Conflict of interest

The authors declare no conflict of interest.

Author details

Hongwei Tan[1], Gang Liu[2,3]* and Run-Wei Li[2,3]

*Address all correspondence to: liug@nimte.ac.cn

1 Nanospin, Department of Applied Physics, Aalto University School of Science, Aalto, Finland

2 CAS Key Laboratory of Magnetic Materials and Devices, Ningbo Institute of Materials Technology and Engineering, Chinese Academy of Sciences, Ningbo, P.R. China

3 Zhejiang Province Key Laboratory of Magnetic Materials and Application Technology, Ningbo Institute of Materials Technology and Engineering, Chinese Academy of Sciences, Ningbo, P.R. China

References

[1] Assefa S, Xia F, Vlasov YA. Reinventing germanium avalanche photodetector for nanophotonic on-chip optical interconnects. Nature. 2010;**464**:80-84. DOI: 10.1038/nature 08813

[2] Assefa S, Shank S, Green W, Khater M, Kiewra E, Reinholm C, Kamlapurkar S, Rylyakov A, Schow C, Horst F, Pan H, Topuria T, Rice P, Gill D M, Rosenberg J, Barwicz T, Yang M, Proesel J, Hofrichter J, Offrein B, Gu X, Haensch W, Ellis-Monaghan J, Vlasov Y. A 90 nm CMOS integrated nano-photonics technology for 25 Gbps WDM optical communication applications. In: IEEE International Electron Devices Meeting (IEDM); Dec 10–13, 2012; San Francisco. Indianapolis, Indiana, U.S.: IBM Press, IEEE; 2012. pp. 33.8.1-33.8.3

[3] Xu Q, Schmidt B, Pradhan S, Lipson M. Micrometre-scale silicon electro-optic modulator. Nature. 2005;**435**:325-327. DOI: 10.1038/nature03569

[4] Liu M, Yin X, Ulin-Avila E, Geng B, Zentgraf T, Ju L, Wang F, Zhang X. A graphene-based broadband optical modulator. Nature. 2011;**474**:64-67. DOI: 10.1038/nature10067

[5] Hosseini P, Wright CD, Bhaskaran H. An optoelectronic framework enabled by low-dimensional phase-change film. Nature. 2014;**511**:206-211. DOI: 10.1038/nature13487

[6] Sun C, Wade MT, Lee Y, Orcutt JS, Alloatti L, Georgas MS, Waterman AS, Shainline JM, Avizienis RR, Lin S, Moss BR, Kumar R, Pavanello F, Atabaki AH, Cook FM, Ou AJ, Leu JC, Chen Y, Asanović K, Ram RJ, Popcvic MA, Stojanović VM. Single-chip microprocessor that communicates directly using light. Nature;**528**:534-538. DOI: 10.1038/nature16454

[7] Sorianello V, Midrio M, Contestabile G, Asselberghs I, Van Campenhout J, Huyghebaert C, Goykhman I, Ott AK, Ferrari AC, Romagnoli M. Graphene-silicon phase modulators with gigahertz bandwidth. Nature Photonics. 2018;**12**:40-44. DOI: 10.1038/s41566-017-0071-6

[8] Ríos C, Stegmaier M, Hosseini P, Wang D, Scherer T, Wright CD, Bhaskaran H, Pernice WHP. Integrated all-photonic non-volatile multi-level memory. Nature Photonics. 2015; **9**:725-732. DOI: 10.1038/NPHOTON.2015.182

[9] Bruck R, Mills B, Troia B, Thomson DJ, Gardes FY, Hu Y, Mashanovich GZ, Passaro VMN, Reed GT, Muskens OL. Device-level characterization of the flow of light in integrated photonics circuits using ultrafast photomodulation spectroscopy. Nature Photonics. 2015;**9**:54-60. DOI: 10.1038/NPHOTON.2014.274

[10] Liu L, Kumar R, Huybrechts K, Spuesens T, Roelkens G, Geluk E, Vries T, Regreny P, Van Thourout D, Baets R, Morthier G. An ultra-small, low-power, all-optical flip-flop memory on a silicon chip. Nature Photonics. 2010;**4**:182-187. DOI: 10.1038/NPHOTON.2009.268

[11] Chua LO. Memristor – The missing circuit element. IEEE Transaction on Circuit Theory. 1971;**18**:507-519

[12] Chua LO, Kang SM. Memristive devices and system. Proceedings of the IEEE. 1976;**64**: 209-223

[13] Strukov DB, Snider GS, Stewart DR, Williams RS. The missing memristor found. Nature. 2008;**453**:80-83. DOI: 10.1038/nature06932

[14] Yang JJ, Pickett MD, Li X, Ohlberg DAA, Stewart DR, Williams RS. Memristive switching mechanism for metal/oxide/metal nanodevices. Nature Nanotechnology. 2008;**3**:429-433. DOI: 10.1038/nnano.2008.160

[15] Szot K, Speier W, Bihlmayer G, Waser R. Switching the electrical resistance of individual dislocation in single-crystalline $SrTiO_3$. Nature Materials. 2006;**5**:312-320. DOI: 10.1038/nmat1614

[16] Waser R, Aono M. Nanoionics-based resistive switching memories. Nature Materials. 2007;**6**:833-840. DOI: 10.1038/nmat2023

[17] Ynag JJ, Strukov DB, Stewart DR. Memristive devices for computing. Nature Nanotechnology. 2013;**8**:13-24. DOI: 10.1038/NNANO.2012.240

[18] Bessonov AA, Kirikova MN, Petukhov DI, Allen M, Ryhänen T, Bailey MJA. Layered memristive and memcapacitive switches for printable electronics. Nature Materials. 2015;**14**:199-204. DOI: 10.1038/NMAT4135

[19] Pan F, Gao S, Chen C, Song C, Zeng F. Recent progress in resistive random access memories: Materials, switching mechanism, and performance. Materials Science and Engineering R. 2014;**83**:1-59. DOI: 10.1016/j.mser.2014.06.002

[20] Zidan MA, Strachan JP, Lu WD. The future of electronics based on memristive systems. Nature Electronics. 2018;**1**:22-29. DOI: 10.1038/s41928-017-0006-8

[21] Borghetti J, Snider GS, Kuekes PJ, Yang JJ, Stewart DR, Williams RS. 'Memristive' switches enable 'stateful' logic operations via materials implication. Nature. 2010;**464**:873-876. DOI: 10.1038/nature08940

[22] You T, Shuai Y, Luo W, Du N, Bürger D, Skorupa I, Hübner R, Henker S, Mayr C, Schüffny R, Mikolajick T, Schmidt OG, Schmidt H. Exploiting memristive $BiFeO_3$ bilayer structures for compact sequential logics. Advanced Functional Materials. 2014;**24**:3357-3365. DOI: 10.1002/adfm.201303365

[23] Xia Q, Robinett W, Cumbie MW, Banerjee N, Cardinali TJ, Yang JJ, Wu W, Li X, Tong WM, Strukov DB, Snider GS, Medeiros-Ribeiro G, Williams RS. Memristor-CMOS hybrid integrated circuits for reconfigurable logic. Nano Letters. 2009;**9**:3640-3645. DOI: 10.1021/nl901874j

[24] Prinz GA. Magnetoelectronics. Science. 1998;**282**:1660-1663. DOI: 10.1126/science.282.5394.1660

[25] Zhou Y, Li Y, Xu L, Zhong S, Sun H, Miao X. 16 Boolean logics in three steps with two anti-aerially connected memristors. Applied Physics Letters. 2015;**106**:233502. DOI: 10.1063/1.4922344

[26] Gao S, Zeng F, Wang M, Wang G, Song C, Pan F. Implementation of complete Boolean logic functions in single complementary resistive switch. Scientific Reports. 2015;**5**:15467. DOI: 10.1038/srep15467

[27] Mathieson K, Loudin J, Goetz G, Huie P, Wang L, Kamins TI, Galambos L, Smith R, Harris JS, Sher A, Palanker D. Photovoltaic retinal prosthesis with high pixel density. Nature Photonics. 2012;**6**:391-397. DOI: 10.1038/NPHOTON.2012.104

[28] Tee BCK, Chortos A, Berndt A, Nguyen AK, Tom A, McGuire A, Lin ZC, Tien K, Bae W, Wang H, Mei P, Chou H, Cui B, Deisseroth K, Ng TN, Bao Z. A skin-inspired organic digital mechanoreceptor. Science. 2015;**350**:313-316. DOI: 10.1126/science.aaa9306

[29] Li H, Zhan Q, Liu Y, Liu L, Yang H, Zuo Z, Shang T, Wang B, Li R-W. Stretchable spin valve with stable magnetic field sensitivity by ribbon-patterned periodic wrinkles. ACS Nano. 2016;**10**:4403-4409. DOI: 10.1021/acsnano.6b00034

[30] Qi D, Liu Z, Liu Y, Jiang Y, Leow WR, Pal M, Pan S, Yang H, Wang Y, Zhang X, Yu J, Li B, Yu Z, Wang W, Chen X. Highly stretchable, compliant, polymeric microelectrode arrays for in vivo electrophysiological interfacing. Advanced Materials. 2017;**29**:1702800. DOI: 10.1002/adma.201702800

[31] Son D, Lee J, Qiao S, Ghaffari R, Kim J, Lee JE, Song C, Kim SJ, Lee DJ, Jun SW, Yan S, Park M, Shin J, Do K, Lee M, Kang K, Hwang CS, Lu N, Hyeon T, Kim D-H. Multifunctional wearable devices for diagnosis and therapy of movement disorders. Nature Nanotechnology. 2014;**9**:397-404. DOI: 10.1038/NNANO.2014.38

[32] Pan C, Dong L, Zhu G, Niu S, Yu R, Yang Q, Liu Y, Wang ZL. High-resolution electroluminescent imaging of pressure distribution using a piezoelectric nanowire LED array. Nature Photonics. 2013;**7**:752-758. DOI: 10.1038/NPHOTON.2013.191

[33] Xue W, Xiao W, Shang J, Chen X, Zhu X, Pan L, Tan H, Zhang W, Ji Z, Liu G, Xu X, Ding J, Li R-W. Intrinsic and interfacial effect of electrode metals on the resistive switching behaviors of zinc oxide films. Nanotechnology. 2014;**25**:425204. DOI: 10.1088/0957-4484/25/42/425204

[34] Majumdar S, Chen B, Qin QH, Majumdar HS, van Dijken S. Electrode dependence of tunneling electroresistance and switching stability in organic ferroelectric P(VDF-TrFE)-based tunnel junctions. Advanced Functional Materials. 2017:1703273. DOI: 10.1002/adfm.201703273

[35] Zhu X, Su W, Liu Y, Hu B, Pan L, Lu W, Zhang J, Li R-W. Observation of conductance quantization in oxide-based resistive switching memory. Advanced Materials. 2012;**24**:3941-3946. DOI: 10.1002/adma.201201506

[36] Peng S, Zhuge F, Chen X, Zhu X, Hu B, Pan L, Chen B, Li R-W. Mechanism for resistive switching in an oxide-based electrochemical metallization memory. Applied Physics Letters. 2012;**100**:072101. DOI: 10.1063/1.3683523

[37] Hu B, Quhe R, Chen C, Zhuge F, Zhu X, Peng S, Chen X, Pan L, Wu Y, Zheng W, Yan Q, Lu J, Li R-W. Electrically controlled electron transfer and resistance switching in reduced graphene oxide noncovalently functionalized with thionine. Journal of Materials Chemistry. 2012;**22**:16422-16430. DOI: 10.1039/c2jm32121a

[38] Hu B, Zhu X, Chen X, Pan L, Peng S, Wu Y, Shang J, Liu G, Yan Q, Li R-W. A multilevel memory based on proton-doped polyazomethine with an excellent uniformity in

resistive switching. Journal of the American Chemical Society. 2012;**134**:17408-17411. DOI: 10.1021/ja307933t

[39] Zhu X, Shang J, Li R-W. Resistive switching effects in oxide sandwiched structures. Frontier of Materials Science. 2012;**6**:183-206. DOI: 10.1007/s11706-012-0170-8

[40] Shang J, Liu G, Yang H, Zhu X, Chen X, Tan H, Hu B, Pan L, Xue W, Li R-W. Thermally stable transparent resistive random access memory based on all-oxide heterostructures. Advanced Functional Materials. 2014;**24**:2171-2179. DOI: 10.1002/adfm.201303274

[41] Pan L, Ji Z, Yi X, Zhu X, Chen X, Shang J, Liu G, Li R-W. Metal-organic framework Nanofilm for mechanically flexible information storage applications. Advanced Functional Materials. 2015;**25**:2677-2685. DOI: 10.1002/adfm.201500449

[42] Pan L, Liu G, Li H, Meng S, Han L, Shang J, Chen B, Platero-Prats AE, Lu W, Zou X, Li R-W. A resistance-switchable and ferroelectric metal−organic framework. Journal of the American Chemical Society. 2014;**136**:17477-17483. DOI: 10.1021/ja508592f

[43] Chen C, Gao S, Tang G, Fu H, Wang G, Song C, Zeng F, Pan F. Effect of electrode materials on AlN-based bipolar and complementary resistive switching. ACS Applied Materials & Interfaces. 2013;**5**:1793-1799. DOI: 10.1021/am303128h

[44] Zhu X, Lee J, Lu WD. Iodine vacancy redistribution in organic–inorganic halide perovskite films and resistive switching effects. Advanced Materials. 2017;**29**:1700527. DOI: 0.1002/adma.201700527

[45] Zhu X, Lu WD. Optogenetics-inspired tunable synaptic functions in memristors. ACS Nano. 2018;**12**:1242-1249. DOI: 10.1021/acsnano.7b07317

[46] Lee M, Lee CB, Lee D, Lee SR, Chang M, Hur JH, Kim Y, Kim C, Seo DH, Seo S, Chung U, Yoo I, Kim K. A fast, high-endurance and scalable non-volatile memory device made from asymmetric Ta_2O_{5-x}/TaO_{2-x} bilayer structures. Nature Materials. 2011;**10**:625-630. DOI: 10.1038/NMAT3070

[47] Feng P, Mönch I, Harazim S, Huang G, Mei Y, Schmidt OG. Giant persistent photoconductivity in rough silicon nanomembranes. Nano Letters. 2009;**9**:3453-3459. DOI: 10.1021/nl9016557

[48] Corma A, Atienzar P, García H, Chane-Ching J. Hierarchically mesostructured doped CeO_2 with potential for solar-cell use. Nature Materials. 2004;**3**:394-397. DOI: 10.1038/nmat1129

[49] Peng L, Hu L, Fang X. Low-dimensional nanostructure ultraviolet photodetectors. Advanced Materials. 2013;**25**:321-5328. DOI: 10.1002/adma.201301802

[50] Chen J, Chiu Y, Li Y, Chueh C, Chen W. Nonvolatile perovskite-based photomemory with a multilevel memory behavior. Advanced Materials. 2017;**29**:1702217. DOI: 10.1002/adma.201702217

[51] Xia F, Wang H, Xiao D, Dubey M, Ramasubramaniam A. Two-dimensional material nanophotonics. Nature Photonics. 2014;**8**:899-907. DOI: 10.1038/NPHOTON.2010.271

[52] Nie R, Deng X, Feng L, Hu G, Wang Y, Yu G, Xu J. Highly sensitive and broadband organic Photodetectors with fast speed gain and large linear dynamic range at low forward bias. Small. 2017;**13**:1603260. DOI: 10.1002/smll.201603260

[53] Ungureanu M, ZazpeR, Golmar F, Stoliar P, Llopis R, Casanova F, Hueso LE. A light-controlled resistive switching memory. Advanced Materials 2012; 24: 2496–2500. DOI: 10.1002/adma.201200382

[54] Bera A, Peng H, Lourembam J, Shen Y, Sun XW, Wu T. A versatile light-switchable nanorod memory: Wurtzite ZnO on Perovskite $SrTiO_3$. Advanced Functional Materials. 2013;**23**:4977-4984. DOI: 10.1002/adfm.201300509

[55] Roy K, Padmanabhan M, Goswami S, Sai TP, Ramalingam G, Raghavan S, Ghosh A. Graphene–MoS_2 hybrid structures for multifunctional photoresponsive memory devices. Nature Nanotechnology. 2013;**8**:826-830. DOI: 10.1038/NNANO.2013.206

[56] Ye C, Peng Q, Li M, Luo J, Tang Z, Pei J, Chen J, Shuai Z, Jiang L, Song Y. Multilevel conductance switching of memory device through photoelectric effect. Journal of the American Chemical Society. 2012;**134**:20053-20059. DOI: 10.1021/ja305354y

[57] Kim YL, Jung HY, Park S, Li B, Liu F, Hao J, Kwon Y, Jung Y, Kar S. Voltage-switchable photocurrents in single-walled carbon nanotube–silicon junctions for analog and digital optoelectronics. Nature Photonics. 2014;**8**:239-243. DOI: 10.1038/NPHOTON.2014.1

[58] Lejman M, Vaudel G, Infante IC, Gemeiner P, Gusev VE, Dkhil B, Ruello P. Giant ultrafast photo-induced shear strain in ferroelectric $BiFeO_3$. Nature Communications. 2014;**5**:4301. DOI: 10.1038/ncomms5301

[59] Ahmadi M, Wu T, Hu B. A review on organic–inorganic halide perovskite photodetectors: Device engineering and fundamental physics. Advanced Materials. 2017;**29**: 1605242. DOI: 10.1002/adma.201605242

[60] Maier P, Hartmann F, Emmerling M, Schneider C, Kamp M, Höfling S, Worschech L. Electro-photo-sensitive memristor for neuromorphic and arithmetic computing. Physical Review Applied. 2016;**5**:054011. DOI: 10.1103/PhysRevApplied.5.054011

[61] Huang Y, Duan X, Cui Y, Lauhon LJ, Kim K, Lieber CM. Logic gates and computation from assembled nanowire building blocks. Science. 2001;**294**:1313-1317. DOI: 10.1126/science.1066192

[62] Bachtold A, Hadley P, Nakanishi T, Dekker C. Logic circuits with carbon nanotube transistors. Science. 2001;**294**:1317-1320. DOI: 10.1126/science.1065824

[63] Joo S, Kim T, Shin SH, Lim JY, Hong J, Song JD, Chang J, Lee H, Rhie K, Han SH, Shin K, Johnson M. Magnetic-field-controlled reconfigurable semiconductor logic. Nature. 2013; **494**:72-76. DOI: 10.1038/nature11817

[64] Terabe K, Hasegawa T, Nakayama T, Aono M. Quantized conductance atomic switch. Nature. 2005;**433**:47-50. DOI: 10.1038/nature03190

[65] Dery H, Dalal P, Cywiski L, Sham LJ. Spin-based logic in semiconductors for reconfigurable large-scale circuits. Nature. 2007;**447**:573-576. DOI: 10.1038/nature05833

[66] Tan H, Liu G, Zhu X, Yang H, Chen B, Chen X, Shang J, Lu WD, Wu Y, Li R-W. An optoelectronic resistive switching memory with integrated demodulating and arithmetic functions. Advanced Materials. 2015;**27**:2797-2803. DOI: 10.1002/adma.201500039

[67] Ney A, Pampuch C, Koch R, Ploog KH. Programmable computing with a single magnetoresistive element. Nature. 2003;**425**:485-487. DOI: 10.1038/nature02014

[68] Tan H, Liu G, Yang H, Yi X, Pan L, Shang J, Long S, Liu M, Wu Y, Li R-W. Light-gated memristor with integrated logic and memory functions. ACS Nano. 2017;**11**:11298-11305. DOI: 10.1021/acsnano.7b05762

[69] Thakoor S, Moopenn A, Daud T, Thakoor AP. Solid-state thin-film memistor for electronic neural networks. Journal of Applied Physics. 1990;**67**:3132-3135. DOI: 0.1063/1.345390

[70] Jo AH, Chang T, Ebong I, Bhadviya BB, Mazumder P, Lu W. Nanoscale memristor device as synapse in neuromorphic systems. Nano Letters. 2010;**10**:1297-1301. DOI: 10.1021/nl904092h

[71] Chang T, Jo S, Lu W. Short-term memory to long-term memory transition in a nanoscale memristor. ACS Nano. 2011;**9**:7669-7676. DOI: 10.1021/nn202983n

[72] Ohno T, Hasegawa T, Tsuruoka T, Terabe K, Gimzewski JK, Aono M. Short-term plasticity and long-term potentiation mimicked in single inorganic synapses. Nature Materials. 2011;**10**:591-595. DOI: 10.1038/NMAT3054

[73] Alibart F, Pleutin S, Bichler O, Gamrat C, Serrano-Gotarredona T, Linares-Barranco B, Vuillaume DA. Memristive nanoparticle/organic hybrid synapstor for neuroinspired computing. Advanced Functional Materials. 2012;**22**:609-616. DOI: 10.100./adfm.20111935

[74] Wang ZQ, Xu HY, Li XH, Yu H, Liu YC, Zhu XJ. Synaptic learning and memory functions achieved using oxygen ion migration/diffusion in an amorphous InGaZnO memristor. Advanced Functional Materials. 2012;**22**:2759-2765. DOI: 10.1002/adfm.201103148

[75] Yu S, Gao B, Fang Z, Yu H, Kang J, Wong HSP. A low energy oxide-based electronic synaptic device for neuromorphic visual systems with tolerance to device variation. Advanced Materials. 2013;**25**:1774-1779. DOI: 10.1002/adma.201203680

[76] Zhu LQ, Wan CJ, Guo LQ, Shi Y, Wan Q. Artificial synapse network on inorganic proton conductor for neuromorphic systems. Nature Communications. 2014;**5**:3158. DOI: 10.1038/ncomms4158

[77] Pickett MD, Medeiros-Ribeiro G, Williams RS. A scalable neuristor built with Mott memristors. Nature Materials. 2013;**12**:114-117. DOI: 10.1038/NMAT3510

[78] Neftci E, Binas J, Rutishauser U, Chicca E, Indiveri G, Douglas RJ. Synthesizing cognition in neuromorphic electronic systems. Proceedings of the National Academy of Sciences of the United States of America. 2013;**110**:E3468-E3476. DOI: 10.1073/pnas.1212083110

[79] Barbera SL, Vuillaume D, Alibart F. Filamentary switching: Synaptic plasticity through device volatility. ACS Nano. 2015;**9**:941-949. DOI: 10.1021/nn506735m

[80] Yang Y, Chen B, Lu WD. Memristive physically evolving networks enabling the emulation of heterosynaptic plasticity. Advanced Materials. 2015;**27**:7720-7727. DOI: 10.1002/adma.201503202

[81] Ignatov M, Ziegler M, Hansen M, Kohlstedt H. Memristive stochastic plasticity enablesmimicking of neural synchrony: Memristive circuit emulates an optical illusion. Science Advances. 2017;**3**:e1700849. DOI: 10.1126/sciadv.1700849

[82] Prezioso M, Merrikh-Bayat F, Hoskins BD, Adam GC, Likharev KK, Strukov DB. Training andoperation of an integrated neuromorphic network based on metal-oxide memristors. Nature. 2015;**521**:61-64. DOI: 10.1038/nature14441

[83] Tan Z, Yang R, Terabe K, Yin X, Zhang X, Guo X. Synaptic metaplasticity realized in oxide memristive devices. Advanced Materials. 2016;**28**:377-384. DOI: 10.1002/adma.201503575

[84] Tuma T, Pantazi A, Gallo ML, Sebastian A, Eleftheriou E. Stochastic phase-change neurons. Nature Nanotechnology. 2016;**11**:693-699. DOI: 10.1038/NNANO.2016.70

[85] Wang Z, Josh S, Savel'ev SE, Jiang H, Midya R, Lin P, Hu M, Ge N, Strachan JP, Li Z, Wu Q, Barnell M, Li G, Xin HL, Williams RS, Xia Q, Yang JJ. Memristors with diffusive dynamics as synaptic emulators for neuromorphic computing. Nature Materials. 2017;**16**:101-108. DOI: 10.1038/NMAT4756

[86] Sheridan PM, Cai F, Du C, Ma W, Zhang Z, Lu WD. Sparse coding with memristor networks. Nature Nanotechnology. 2017;**12**:784-789. DOI: 10.1038/NNANO.2017.83

[87] Kumar S, Strachan JP, Williams RS. Chaotic dynamics in nanoscale NbO_2 Mott memristors for analogue computing. Nature. 2017;**548**:318-321. DOI: 10.1038/nature23307

[88] Lee M, Lee W, Choi S, Jo J, Kim J, Park SK, Kim Y. Brain-inspired photonic neuromorphic devices using photodynamic amorphous oxide semiconductors and their persistent photoconductivity. Advanced Materials. 2017;**29**:1700951. DOI: 10.1002/adma.201700951

[89] Choi C, Choi MK, Liu S, Kim MS, Park OK, Im C, Kim J, Qin X, Lee GJ, Cho KW, Kim M, Joh E, Lee J, Son D, Kwon S, Jeon NL, Song YM, Lu N, Kim D. Human eye-inspired soft optoelectronic device using high-density MoS_2-graphene curved image sensor array. Nature Communications. 2017;**8**:1664. DOI: 10.1038/s41467-017-01824-6

[90] Maya-Vetencourt JF, Ghezzi D, Antognazza MR, Colombo E, Mete M, Feyen P, Desii A, Buschiazzo A, Paolo MD, Marco SD, Ticconi F, Emionite L, Shmal D, Marini C, Donelli I, Freddi G, Maccarone R, Bisti S, Sambuceti G, Pertile G, Lanzani G, Benfenati F. A fully organic retinal prosthesis restores vision in a rat model of degenerative blindness. Nature Materials. 2017;**16**:681-689. DOI: 10.1038/NMAT4874

[91] Ko HC, Stoykovich MP, Song J, Malyarchuk V, Cho WM, Yu C, Geddes III JB, Xiao J, Wang S, Huang Y, Rogers JA. A hemispherical electronic eye camera based on compressible silicon optoelectronics. Nature. 2008;**454**:748-753. DOI: 10.1038/nature07113

[92] Chen S, Lou Z, Chen D, Shen G. An artificial flexible visual memory system based on an UV-motivated memristor. Advanced Materials. 2017;**29**:1705400. DOI: 10.1002/adma.201705400

[93] Yang H, Wang B, Zhu X, Shang J, Chen B, Li R-W. Modulation of physical properties of oxide thin films by multiple fields. Chinese Physics B. 2016;**25**:067303. DOI: 10.1088/1674-1056/25/6/067303

[94] Xue W, Liu G, Zhong Z, Dai Y, Shang J, Liu Y, Yang H, Yi X, Tan H, Pan L, Gao S, Ding J, Xu X-H, Li R-W. A 1D vanadium dioxide nanochannel constructed via electric-field-induced ion transport and its superior metal–insulator transition. Advanced Materials. 2017;**29**:1702162. DOI: 10.1002/adma.201702162

[95] Chen X, Zhu X, Xiao W, Liu G, Feng YP, Ding J, Li R-W. Nanoscale magnetization reversal caused by electric field-induced ion migration and redistribution in cobalt ferrite thin films. ACS Nano. 2015;**9**:4210-4218. DOI: 10.1021/acsnano.5b00456

[96] Zhu X, Zhou J, Chen L, Guo S, Liu G, Li R-W, Lu WD. In situ nanoscale electric field control of magnetism by nanoionics. Advanced Materials. 2016;**28**:7658-7665. DOI: 10.1002/adma.201601425

[97] Yao L, Inkinen S, van Dijken S. Direct observation of oxygen vacancy-driven structural and resistive phase transitions in $La_{2/3}Sr_{1/3}MnO_3$. Nature Communications. 2017;**8**:14544. DOI: 10.1038/ncomms14544

[98] Kim T, McCall JG, Jung YH, Huang X, Siuda ER, Li Y, Song J, Song YM, Pao HA, Kim R, Lu C, Lee SD, Song I, Shin G, Al-Hasani R, Kim S, Tan MP, Huang Y, Omenetto FG, Rogers JA, Bruchas MR. Injectable, cellular-scale optoelectronics with applications for wireless optogenetics. Science. 2013;**340**:211-216. DOI: 10.1126/science.1232437

[99] Wu F, Stark E, Ku P, Wise KD, Buzsaki G, Yoon E. Monolithically integrated uLEDs on silicon neural probes for high-resolution optogenetic studies in behaving animals. Neuron. 2015;**88**:1136-1148. DOI: 10.1016/j.neuron.2015.10.032

[100] Canales A, Jia X, Froriep UP, Koppes RA, Tringides CM, Selvidge J, Lu C, Hou C, Wei L, Flink Y, Anikeeva P. Multifunctional fibers for simultaneous optical, electrical and chemical interrogation of neural circuits *in vivo*. Nature Biotechnology. 2015;**33**:277-284. DOI: 10.1038/nbt.3093